DOKUZ EYLÜL UNIVERSITY
GRADUATE SCHOOL OF NATURAL AND APPLIED SCIENCES

DESIGN AND OPTIMIZATION OF ICE-ON-COIL LATENT THERMAL STORAGE SYSTEM

by
Mehmet Akif EZAN

July, 2006
İZMİR

DESIGN AND OPTIMIZATION OF ICE-ON-COIL LATENT THERMAL STORAGE SYSTEM

A Thesis Submitted to the
Graduate School of Natural and Applied Sciences of
Dokuz Eylül University
In Partial Fulfillment of the Requirements for the Degree of Master of Science in Mechanical Engineering, Thermodynamics Program

by
Mehmet Akif EZAN

July, 2006
İZMİR

M.Sc THESIS EXAMINATION RESULT FORM

We have read the thesis entitled **"DESIGN AND OPTIMIZATION OF ICE-ON-COIL LATENT THERMAL STORAGE SYSTEM"** completed by **MEHMET AKİF EZAN** under supervision of **ASSIST. PROF. Dr. AYTUNÇ EREK** and we certify that in our opinion it is fully adequate, in scope and quality, as a thesis for the degree of Master of Science.

Assist. Prof. Dr. AYTUNÇ EREK

Supervisor

Prof. Dr. ZAFER İLKEN	Assist. Prof. Dr. HÜSEYİN GÜNERHAN
(Jury Member)	(Jury Member)

Prof. Dr. Cahit HELVACI

Director

Graduate School of Natural and Applied Sciences

ACKNOWLEDMENTS

I wish to express my sincere gratitude to my advisor, Ass. Prof. Dr. Aytunç EREK, for providing excellent guidance and constant encouragement throughout the preparation of this work. His contribution to the achievements of this work is significant.

I would also like to thank the technician Alim ZORLUOL providing his expertise to experiments and this thesis.

I also wish to express my gratitude to my friends at the Dept. of Mechanical Engineering for their endless patience, help and support.

Finally, I would like to thank my parents for their encouragements, especially my brother Atıf C. EZAN and all my friends.

Mehmet Akif EZAN

DESIGN AND OPTIMIZATION OF ICE-ON-COIL LATENT THERMAL STORAGE SYSTEM

ABSTRACT

In this thesis study, the effects of various operation conditions to cool storage in latent thermal energy storage system with spiral pipes, is investigated experimentally and the results are compared with the numerical data. The aim of the study is to reveal the optimum operation condition of the thermal energy storage for required cooling load by using the numerical and experimental results. It is exposed that the inlet temperature of the fluid is more influential to increase the energy stored rather than the volumetric flow rate and the numerical code, which basis on enthalpy method, have a good approximation with experimental results for low Reynolds numbers.

Keywords: Phase change, Solidification, Thermal energy storage, Experimental and numerical analysis

SERPANTİN ÜZERİNDE BUZLU GİZLİ ENERJİ DEPOLAMA SİSTEMİNİN TASARIMI VE OPTİMİZASONU

ÖZ

Bu tez çalışmasında, spiral borulu ısıl enerji deposundaki soğu enerjisi depolamasına, değişik çalışma koşullarının etkisi deneysel olarak incelenmiş, elde edilen deneysel sonuçlar ise sayısal yöntemin sonuçlarıyla karşılaştırılmıştır. Bu çalışmanın amacı, elde edilen deneysel ve nümerik sonuçlar ışığında, ısıl enerji depolama sisteminden istenen soğutma yüküne uygun olacak optimum çalışma şartlarının tespit edilmesidir. Akışkan giriş sıcaklığının depolanan enerjiyi arttırmada, hacimsel debiye göre daha etkili olduğu ve entalpi yöntemini temel alan nümerik kodun, düşük Reynolds sayıları için deneysel sonuçlara yakınsadığı ortaya konmuştur.

Anahtar sözcükler: Faz değişimi, Katılaşma, Isıl enerji depolama, Deneysel ve sayısal analiz

CONTENTS

Page

M.Sc THESIS EXAMINATION RESULT FORM ii
ACKNOWLEDMENTS iii
ABSTRACT iv
ÖZ v

CHAPTER ONE – INTRODUCTION 1
1.1 Introduction 1
1.1.1 Sensible Thermal Energy Storage (STES) 2
1.1.2 Latent Thermal Energy Storage (LTES) 2

CHAPTER TWO – EXPERIMENTAL SETUP AND PROCEDURE 12
2.1 Experimental Setup 12

2.2 Metering Systems and Experimental Procedure 16
2.2.1 Metering System 16
2.2.2 Uncertainty Analysis 19

2.3 Determination of The Total Stored Energy 22
2.3.1 Latent Energy 22
2.3.2 Sensible Energy 23
2.3.3 Gained Energy 25

2.4 Experimental Results 26

CHAPTER THREE – MATHEMATICAL FORMULATION AND NUMERICAL MODEL 29
3.1 Introduction 29

3.2 Governing Equations 30
3.2.1 Equations For Heat Transfer Fluid 30

3.2.2 Equations For The Pipe Wall 32
3.2.3 Equations For Phase Change Material (PCM) 34

3.3 Non-dimensional Form of Governing Equations 38
3.3.1 Non-dimensional Form of HTF Equation 39
3.3.2 Non-dimensional Form of Pipe Wall Equation 41
3.3.3 Non-dimensional Form of PCM Equation 41

3.4 The Related Initial and Boundary Conditions 42

3.5 Control-Volume Formulation and Discretization 43

3.6 Discretization of Governing Equations 51
3.6.1 Discretization of HTF Equation 52
3.6.2 Discretization of Pipe Wall Equation 53
3.6.3 Discretization of Pipe Wall – HTF Interface Equation 54
3.6.4 Discretization of PCM Equation 55

3.7 Mathematical Model 57

3.8 Computational Algorithm 58

3.9 Numerical Code Validation 59

3.10 Numerical Results 61

CHAPTER FOUR – CONCLUSIONS 63

REFERENCES 69

APPENDIX 76
A.1 Formulation of the S.I.S. Solver (Lee, 1989) 76

CHAPTER ONE
INTRODUCTION

1.1 Introduction

Energy is the most necessary part of the modern life. Although, the fossil fuel resources are the main elements to gain energy, in terms of economical and environmental facilities, they have become very expensive, they cause lots of environmental pollution and furthermore the reserves are so limited. Hence, in time, it will come to an end. On this account, investigations about alternative energy resources, energy conversation methods and wasting the existing energy more efficiently, have become significant. In this respect, recently, thermal energy storage (TES) has become popular and been adapted in many engineering applications, for storing energy in daily, weekly, monthly or annual periods to use later.

On account of increasing thermal loads in buildings, rising living standards and climatic change, heating and especially cooling is becoming more and more important and the demand on cooling is expanding very quickly around the world. The increased cooling demand results in peak electrical power demand during the hottest summer days. Thermal energy storage (TES) systems not only shift cooling energy to use at non-peak times, but also reduce energy consumption, depending on site-specific design, notably where chillers can be operated at full load during the night.

Thermal energy storage systems are mainly divided into two: *Sensible thermal energy storage (STES)* and *Latent thermal energy storage (LTES)*. In former one, energy is stored by means of the temperature difference of the storage medium and in latter one; energy is stored via using the phase change energy of the storage medium.

1.1.1 Sensible Thermal Energy Storage (STES)

Sensible energy storage is simply defined as, *heat storage or cool storage in which all of the energy stored is in the form of sensible heat associated with a temperature change in the storage medium*, in ASHRAE (1999). In sensible energy storage systems, the heat storage medium has to have some features, such as; high heat capacity, thermal stability under long periods of cycles, environmentally benign, low cost and availability.

In sensible energy storage systems, *solids* or *liquids* can be used as storage medium. Fluids that are widely used as liquid medium can be listed as; water, salt water, petroleum based oils, and etc. Nevertheless, water is one of the best medium in liquids for sensible energy storage, with its high heat capacity, low cost and availability. On account of high vapour pressure, liquid mediums are commonly used for low temperature applications –temperatures between the freezing and boiling temperatures– such as; water heating, space heating and air conditioning. Rocks, metals and bricks are the most common materials used as solid medium in sensible energy storage systems. Solid materials can be used for low or high temperature applications, since these materials do not have any difficulty such as freezing or boiling. In comparison with liquids, solids have low heat capacity and they are relatively more expensive, so only the massive stones are preferred in commercial use.

1.1.2 Latent Thermal Energy Storage (LTES)

Latent energy storage is simply defined as, *heat storage or cool storage in which the energy is largely as latent heat associated with a phase change in the storage medium*, in ASHRAE (1999). Latent energy storage systems are efficient solutions for reducing the demand of energy and recently these systems have been used for commercial applications. In comparison with the other energy storing methods, there exist many advantages of the latent energy storage, such as having high ratio of

energy / volume and less phase change material usage to store high amount of energy in a narrow temperature band.

As an illustration, heat requires to melt 1kg of ice is 80 times greater than the heat to increase temperature of 1 kg water to 1˚C. Phase change materials (PCMs) that are commonly used can make solid-to-liquid or liquid-to-vapour phase transforms. Liquid-to-vapour phase change produces very high energy; nevertheless, liquid-to-vapour phase change is not widely used because of high volume change in constant pressure or high pressure change in constant volume. Solid-to-liquid phase change is more useful than the other phase change methods with the advantage of storing very high energy at narrow temperature interval with less volume change.

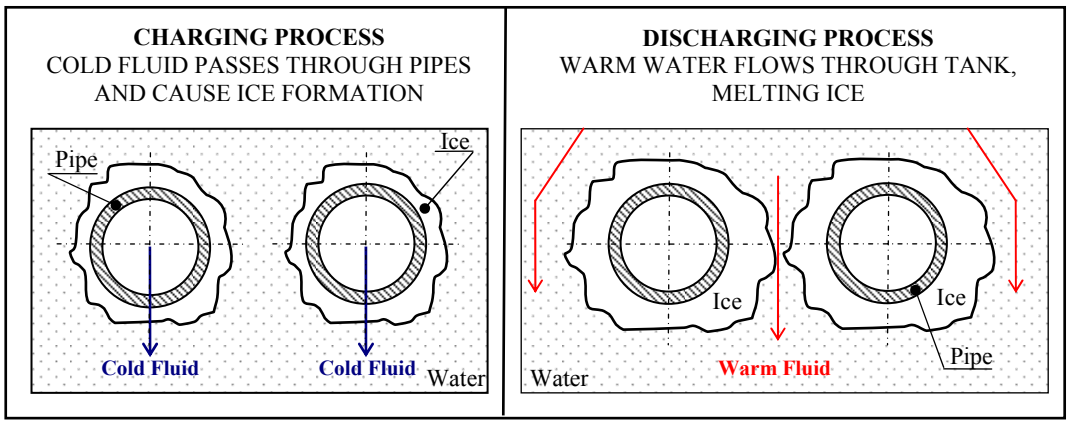

(a) External melting ice storage

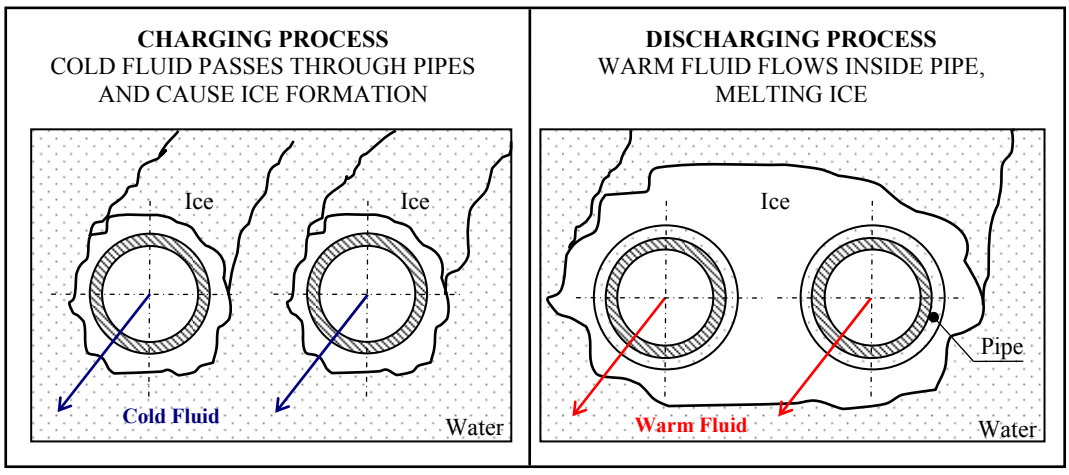

(b) Internal melting ice storage

Figure 1.1 Charge and discharge of melt ice storage

Figure 1.1 illustrates both charge and discharge methods of melt ice storage, in two ways; internal or external.

There are many materials that can be use as storage medium for solid-to-liquid phase change. Materials has to have some features to use as PCM and ASHRAE (1999) determines these features as,

- Available
- Cheap
- Environmentally benign
- None explosive
- None corrosion or abrasive
- Well documented thermal and physical characteristics
- High density
- High heat of fusion
- High heat capacity
- Suitable thermal and physical characteristics for long time use

Under these circumstances, the most useful phase change materials are; water, various brine mixes, salty hydrate, organic and inorganic materials like paraffin and polyethylene glycol. Water covers all of the features listed above, consequently, it is the most common and accepted material for the latent energy storage systems, as PCM medium.

In latent energy storage systems, energy can be stored as heat or cool at PCM. For instance, charging solar energy in daytime and discharging it at night or after long periods for residence or greenhouse heating, storing solar energy in space stations and using that energy in shadowed positions in space (Vakilaltojjar et al., 2001) are some applications of *latent heat storage*. On the other hand, *latent cool storage* is widely used in air conditioning system. Cool is stored at times –e.g. nighttime– while the electrical energy is cheap, and then it can be used later –e.g. daytime, when the

electrical energy is relatively expensive. By this way, many advantages occur as discussed below.

The electrical energy demand variation of a conventional air conditioning system through a day is illustrated in Figure 1.2a. The energy costs for cooling a building increase depending on the high demand of energy in certain periods of day. Cool storage unit can be added into the system to produce ice at nighttime when electrical energy costs are relatively low and use this stored energy at daytime. This will balance load distribution throughout the day as shown in Figure 1.2b. By means of reducing high-energy costs and peak load, the capacity of hardware, damage of installation and dimensions of existing systems will reduce noteworthy (ASHRAE, 1999; Dincer and Rosen, 2002). Reduction in dimensions of distribution pipes and system installations reveal more usable space in buildings. *Sometimes these spaces are enough to build an extra floor* (ASHRAE, 1999). By means of energy suppliers, instead of using their resources for new installations or purchasing new equipments to provide the increasing demand of energy, manufacturers can transfer their current funds to improve efficiency of their existing systems.

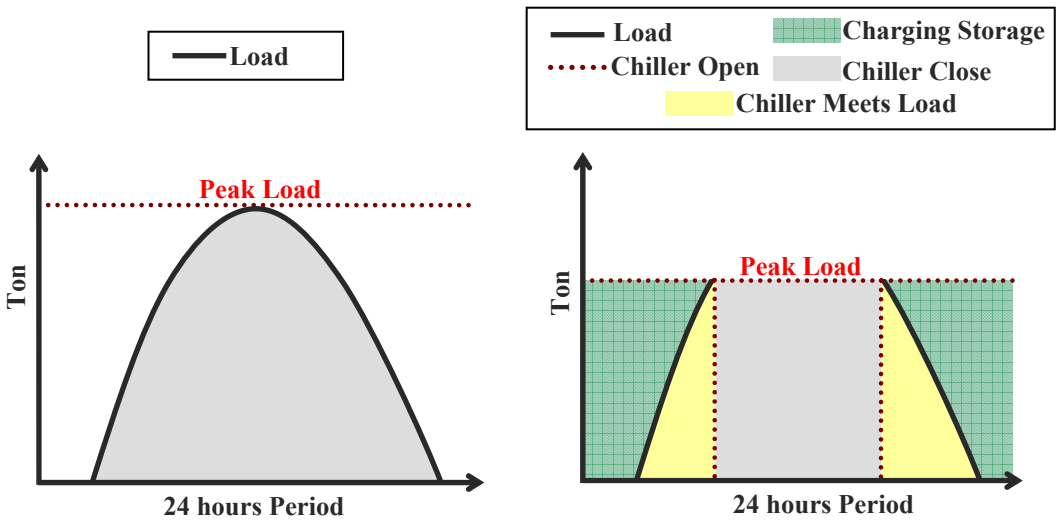

(a) (b)

Figure 1.2 Daytime load distribution of air conditioning unit (a) without cool storage (b) with cool storage

Another advantage of the thermal energy storage is the ability of using energy more efficiently. Storing energy at nighttime, when the ambient temperature is relatively less than the daytime, is more efficient for the system because of the low temperature of fluid, which enters to the condenser. In summer time, the system works at a condensing temperature, which is 20˚C less than the daytime, that cause 2-3 % more efficient usage compared to a system working throughout the day without energy storage (Erek et al., 2005[a]).

In addition to the economical advantages of the latent energy storage applications, there are also some environmental benefits. Recently, energy is widely obtained from fossil fuels, which are known to have negative effects and be very harmful for the environment. Fossil fuel usage will seriously reduce, while the energy storage applications become widespread, which will diminish energy requirement and ensure using energy more efficiently (Dincer and Rosen, 2002). Moreover, it is certain that chillers use CFC type gases, as refrigerant fluids, which are harmful for the environment and especially for the Ozone layer. Assembling the latent energy storage systems to certain HVAC systems will reduce existing cooling capacities; hence CFC emissions and their damages to the environment will also be reduced.

Because of the reasons above mentioned, recently, storing latent energy problem for cooling systems (also named as phase change problem) has become popular and investigations about this phenomena is supported with both numerical and experimental studies. Because of its complexity, the phase change problems have a limited number of analytical solutions. Most of the available solutions are for simplified and idealized one-dimensional systems.

A lot of mathematical models have been developed to simulate the ice-on-coil storage systems with external and internal melt and some of them have been supported by the experimental studies. Jekel et al. (1993) and Nelson et al. (1996) have developed a model and studied an internal melt ice-on-coil system during charge and discharge process. Neto and Krarti (1997[a], 1997[b]) described a dynamic model for an internal melt ice-on-coil thermal storage tank, based on a quasi steady-

state analysis and a thermal resistance network technique. Zhu and Zhang (2001) have investigated the effect of ice-water density difference on internal melt ice-on-coil thermal energy storage system. Trp (2005) developed a complete model using enthalpy formulation for external melt on coil. Lee and Jones (1996) developed a stand-along analytical model for an ice-on-coil thermal energy storage system with both charging and discharging modes, and validated the numerical results with the experimental ones. Numerical simulations have been performed to investigate the effect of flow parameters and compared with experimental results in an ice-on-coil system (Erek et al., 2005[a]).

In literature, studies that are concerned with the latent energy storage systems, are focused on three main topics (Zalba et al., 2003)

- Phase Change Materials (PCM)
- Heat Transfer Analysis
- Applications

1.1.2.1 Phase Change Material (PCM)

There are many materials to be used in latent energy storage systems. Many studies made on the application of the phase change materials for the latent energy storage systems (Abhat, 1983; Farid et al., 2005; Humphries, 1977; Lane et al., 1975; Lorsch et al., 1976; Vakilaltojjar et al., 2001). Phase change materials must provide some features such as, having high heat of fusion and thermal conductivity, being stable –no change of properties during thermal cycles– including no harmful components for humans or the environment, being cheap and commonly available. Phase change materials can be used to store heat or cool in latent energy storage systems. Usage of PCM is determined from its melting temperature. Materials melting under 15˚C are suitable for cool storage in air conditioning systems and materials dissolving over 90˚C are suitable for cooling systems with absorption (Farid et al., 2005). Table 1.1 shows the thermo-physical properties of the most

common used phase change materials for their solid and liquid phases (Farid et al., 2005).

For the latent energy storage applications, water is the most common and accepted material, with high heat of fusion and stability under long cycles.

Table 1.1 Thermo-physical properties of some materials in solid and liquid phases (Farid et al., 2005, Zalba et al., 2003)

Material	**Melting Temperature**	**Latent Heat**	**Thermal Conductivity**	**Density**
	(˚C)	(kJ/kg)	(W/mK)	(kg/m^3)
H_2O (Zalba)	0	334	0.612 (liquid, 20˚C)	998 (liquid, 20˚C) 917 (solid, 0˚C)
Inorganic				
$MgCl_2•6H_2O$	117	168.6	0.570 (liquid, 120˚C) 0.694 (solid, 90˚C)	1450 (liquid, 120˚C) 1569 (solid, 20˚C)
$Mg(NO_3)_2•6H_2O$	89	162.8	0.490 (liquid, 95˚C) 0.611(solid, 37˚C)	1550 (liquid, 94˚C) 1636 (solid, 25˚C)
$Ba(OH)_2•8H_2O$	48	265.7	0.653 (liquid, 85.7˚C) 1.225 (solid, 23˚C)	1937 (liquid, 84˚C) 2070 (solid, 24˚C)
$CaCl_2•6H_2O$	29	190.8	0.540 (liquid, 38.7˚C) 1.088 (solid, 23˚C)	1562 (liquid, 32˚C) 1802 (solid, 24˚C)
Organic				
Parafin	64	173.6	0.167 (liquid, 63.5˚C) 0.346 (solid, 33.6˚C)	790 (liquid, 65˚C) 916 (solid, 24˚C)
Polyglycol E600	22	127.2	0.189 (liquid, 38.6˚C)	1126 (liquid, 25˚C) 1232 (solid, 4˚C)
Fatty Acids				
Palmitic acid	64	185.4	0.162 (liquid, 68.4˚C)	850 (liquid, 65˚C) 989 (solid, 24˚C)
Capric acid	32	152.7	0.153 (liquid, 38.5˚C)	878 (liquid, 45˚C) 1004 (solid, 24˚C)
Caprylic acid	16	148.5	0.149 (liquid, 38.6˚C)	901 (liquid, 30˚C) 981 (solid, 13˚C)
Aromatics				
Naphthalene	80	147.7	0.132 (liquid, 83.8˚C) 0.341 (solid, 49.9˚C)	976 (liquid, 84˚C) 1145 (solid, 20˚C)

1.1.2.2 Heat Transfer Analysis

Recently, many companies have represented their modular latent heat storage systems and these systems are widely used in applications successfully (Ismail et al.,

1999). Meanwhile, many experimental and theoretical studies are carried on that aims to improve current technology. In literature, there are many resources about heat transfer mechanism, formulation, solution methods and new models to simulate the phase change phenomenon.

A classical phase change problem, called as "*Neumann problem"*, is a semi-infinite region of constant initial temperature T_i, and the temperature of its surface is suddenly dropped and held at a constant temperature T_w. Neumann derived an analytical solution to this problem by using a similarity transformation. The obtained solution is valid for constant properties, constant temperature boundary conditions and isothermal phase change. If the initial temperature of the Neumann problem is equal to the phase change temperature, T_m, then the problem is called as "*Stefan problem*" after Stefan, who obtained an approximate solution to the error function (Ismail and Abugderah, 2000).

A number of studies have been conducted to analyze the thermal behavior of latent heat thermal energy storage systems. Studies related to the shell-and-tube type of exchanger configuration have been carried out by Bellecci and Conti (1993), Cao and Faghri (1991[a]), Cao and Faghri (1991[b]), Ismail and Alves (1986), Lacroix (1993), and Zhang and Faghri (1996). It has been determined that the shell-and-tube type heat exchanger is the most promising device as a latent energy storage system that requires high efficiency for a minimum volume. In such an energy storing unit, the phase change material (PCM) fills the gap between the shell and the tubes in which heat transfer fluid (HTF) flows, also serves to convey the stored energy to and from the unit. Recently, a theoretical model of the shell-and-tube type unit for storing energy has been reported by Ismail and Alves (1986). In addition, Cao and Faghri (1991[b], 1992) have also modeled a similar problem at which both the heat charging and the recovery processes have been performed by the circulating fluid. For both models, the shell wall of the unit was assumed to be adiabatic. Using the enthalpy model, the problem of storing energy in a shell-and-tube type unit was also solved by Bellecci and Conti (1993). Cao and Faghri (1991[a]) have studied the latent heat energy storage systems for both annular and countercurrent flows and numerically

determined that the storage system with the countercurrent flow was an efficient way to absorb heat energy.

1.1.2.3 Applications

There exist different types of applications about the thermal energy storage systems. Table 1.2 gives an overview about some of these applications with references. Dincer and Rosen (2002) explain further information about the applications of TES (latent TES, cold TES and seasonal TES). There are also some corporations about TES systems, such as *CALMAC*, *Cristopia*, *Baltimore Air Coil*, *Cryogel* and etc., web cites concerned with these TES corporations are listed in references.

Ice-on-coil thermal energy storage technology has been used for many years in various types of applications. Furthermore, these systems can be easily adapted to conventional systems with using the modular cool storage units.

Table 1.2 PCM and Thermal energy storage applications (Zalba et al., 2003)

Application	**References**
Thermal storage of solar energy	(Lane, 1986)
Passive storage in bioclimatic building/architecture (HDPE + paraffin)	(Hawes et al., 1993)
Cooling: use of off-peak rates and reduction of installed power, ice-bank	(Ismail et al., 2001)
Heating and sanitary hot water: using off-peak rate and adapting unloading curves	(Farid et al., 1990)
Thermal protection of food: transport, hotel trade, ice-cream, etc.	(Espeau et al., 1997)
Thermal protection of electronic devices (integrated in the appliance)	(Cabeza et al., 2002)
Medical applications: transport of blood, operating tables, hot-cold therapies	(Cabeza et al., 2002)
Cooling engines (electric and combustion)	(Pal et al., 1997)
Softening of exothermic temperature peaks in chemical reactions	(Salyer et al., 1990)
Spacecraft thermal systems	(Mulligan et al.,1996)
Solar power plants	(Michels et al., 1996)

This research study deal with the thermal energy storage both experimentally and numerically. For an ice-on-coil latent thermal energy storage system, the effects of various inlet conditions of coolant, such as flow rate and temperature, on charging process is investigated experimentally and a numerical code is adapted to simulate

the system which can be use to achieve design and manufacturing parameters for any new LTES system. In literature, most of the experimental studies related with the solidification around only single pipe and results comprised with numerical methods, developed by researcher. Here, the experimental setup consists of a whole climate unit, with lots of pipes and the results are obtained for entire system, and the results of which are validated by using the numerical model conducted by Erek (1999, 2005[b]), which includes temperature transforming model for PCM and quasi-steady assumption for the heat transfer fluid.

The following chapter of the thesis is the expression of the experimental study, with its results and discussions. The third chapter of the thesis describes numerical assumptions for the phase change problem, its governing equations, solution methodologies, algorithms and the results. As a conclusion, the last chapter represents the comparative results and their concluding remarks.

CHAPTER TWO
EXPERIMENTAL SETUP AND PROCEDURE

2.1 Experimental Setup

An experimental latent thermal energy storage unit, as shown in Figure 2.1 and Figure 2.2, was constructed to perform the experimental analysis. The system includes a chiller integrated with a cool storage tank. The storage tank is filled with water, in which there is a submerged polyethylene tube bundle. Ethylene glycol-water solution (40 % of ethylene glycol in volume concentration) is cooled by the chiller and pumped through the tubes using *inlet* and *outlet collectors*. Thus, the brine freezes the water surrounding the tubes. During the discharge period, cold water is collected using a *water outlet* connection and it is circulated to meet a cooling demand. Afterwards relatively warm water is returned to the top of the ice storage tank using *water inlet* connection. In addition, during the discharge period, by injecting air at the bottom of the tank using the *air inlet* connection, air bubbles promote a uniform and quicker melting process when required. *Water discharge* and *overflow* connections are designed to enable the discharge of the tank and overflowing.

Ethylene glycol-water solution is pumped through eight polyethylene tubes using *collectors*. The internal and external diameters of the tubes are 13 mm and 17 mm, respectively. *Polyethylene tubes* which are 13 m of total length are connected by the *supporting construction*. By considering ice formulation at the end of the charge process, the spacing between the tubes was determined from the numerical study. Spiral pipe construction can be seen in Figure 2.1. Counter-flow provides the ice to be built uniformly throughout the cross section of the cool storage tank. Thus, the tank volume can be used more effectively. Excluding the ice surrounding the tubes, cooled water around freezing point in the tank was collected by the *water outlet* tubes placed at the bottom of the cool storage tank. After circulation for cooling some volume, relatively warm water is pumped through the *water inlet* tubes. *Air inlet* tubes are placed at the bottom of the tank for injecting pressurized air. The

whole tank is insulated with foam rubber insulation (*4 cm thick* with $k = 0.038$ *W/mK*).

Experimental setup is shown in Figure 2.2a, with the chiller set on the right side and the storage tank is on the other side, connected with the pump system. And also, the spiral pipes and the ice formation around after 12 hours can be seen in Figure 2.2b.

Table 2.1 Thermo-physical properties of HTF, PCM and tube wall

Material		ρ (kg.m^{-3})	c_p (J.kg^{-1}.K^{-1})	k (W.m^{-1}.K^{-1})	α (m^2.s^{-1})	μ (mPa.s)	ΔH (J.kg^{-1})
HTF (%40) Ethylene Glycol *	-5˚C	1066.80	3401	0.389	1.072x10^{-7}	7.18	–
	-10˚C	1068.28	3384	0.383	1.059x10^{-7}	9.06	
	-15˚C	1069.63	3367	0.377	1.047x10^{-7}	11.74	
TUBE WALL Polyethylene		938	2300	0.38	1.761x10^{-7}	–	–
PCM Water	Liquid	999.8	4210	0.567	1.347x10^{-7}	–	–
	Solid	916.8	2040	2.2	1.176x10^{-7}	–	333400

* Source: ASHRAE Fundamentals 1997

The thermo-physical properties of the materials, used in the experiments, are listed in the Table 2.1. Here, properties of the ethylene glycol-water solution is given for a temperature interval, via the inlet temperature of the coolant can not be stable for each experiment, as explained in following sections.

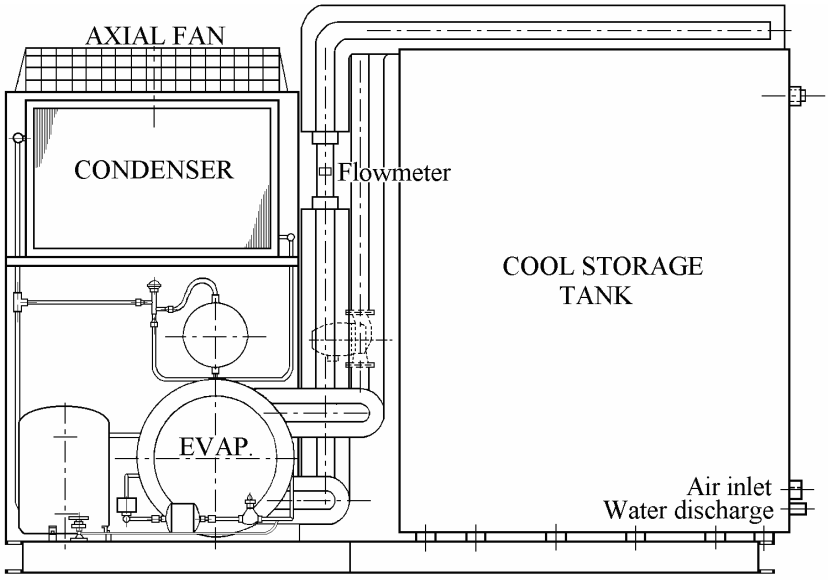

Figure 2.1a Energy storage unit – Refrigerator integrated with storage tank

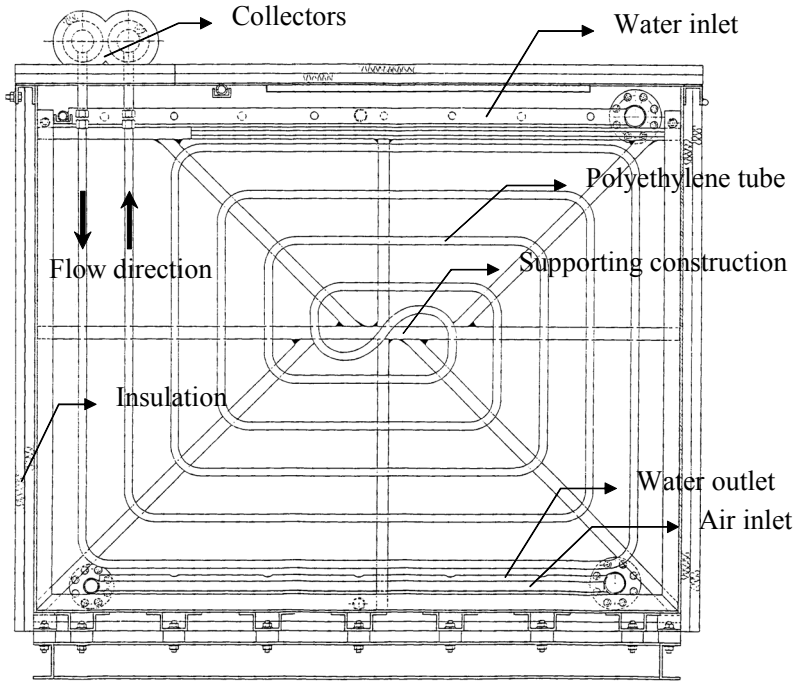

Figure 2.1b Energy storage unit – Construction of the storage tank

Figure 2.2a Experimental setup

Figure 2.2b Ice formation around pipes after 12 Hours

2.2 Metering Systems and Experimental Procedure

2.2.1 Metering System

The secondary fluid (ethylene glycol-water solution) heat transfer rates were determined from the measured temperature difference between the inlet and the outlet collectors and the flow rate of the secondary fluid through the thermal energy storage system. The flow rate of the secondary fluid through the storage tank was measured by using an acrylic tube flow meter. The flow meter has an accuracy of ±0.5 % of full scale. The two type T copper-constantan thermocouples with a standard error of ±1.0°C were measured the inlet and outlet temperatures of the secondary fluid.

A total of 16 thermocouples were installed inside the storage tank to measure the outer surface temperature of tubes carrying the secondary fluid at both inlet and outlet connections through the collectors. Furthermore, two thermocouples at different locations inside the tank are used to measure the water temperature which is used as the phase change material. Hence, totally 20 thermocouples were used to measure the temperature variations of the system.

All thermocouples used in the experiments are type of T with gage no. 24 and were calibrated by using a constant temperature bath, HAAKE model and type T. In the temperature bath, the temperatures were measured by a precision thermometer, and bath was filled with ethyl-alcohol. Thermocouples were immersed inside the ethyl-alcohol and calibrated for a temperature interval of –10°C to 5°C. Hence, the calibration curves for each thermocouple are obtained for an interval of –10°C to 5°C. In each increment of bath temperature, the ethyl-alcohol solution was allowed to reach a steady temperature, and then the precision thermometer and the data logger readings were recorded. Calibration curve of a particular thermocouple is given in Figure 2.3 and the calibration equations for each thermocouple are given in Table 2.2.

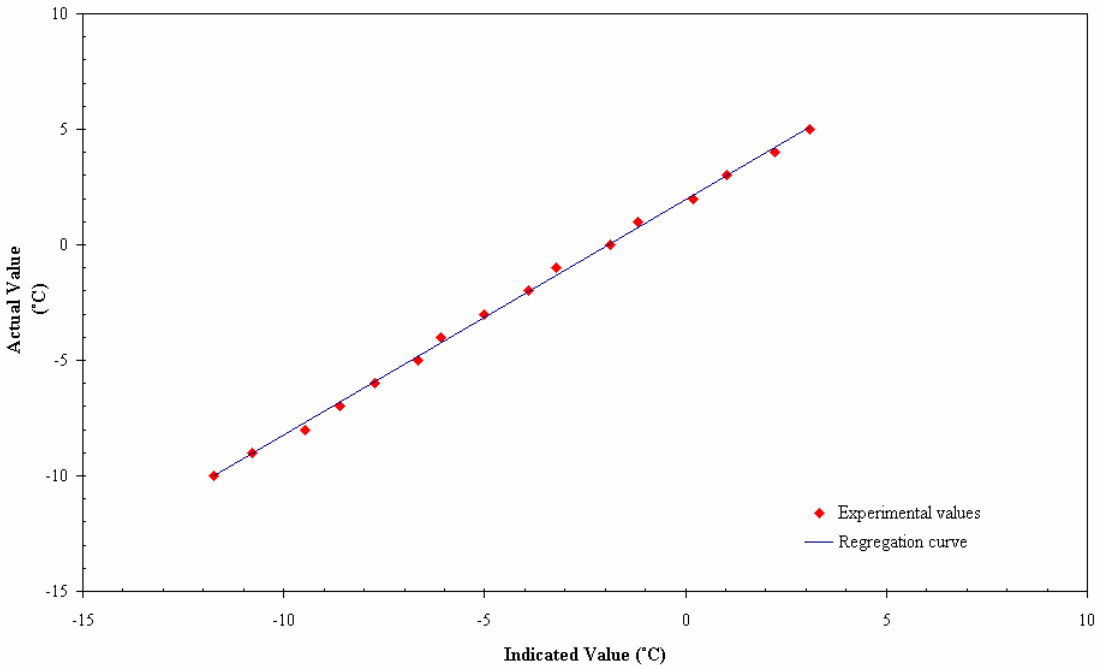

Figure 2.3 Calibration curve of a typical thermocouple wire

An HP type 34970A data logger was used for temperature readings. Data logger has an accuracy of ±0.04 % of the reading. The millivolt outputs of the thermocouples and the measured voltage is automatically converted into temperature and transmitted to a PC.

The temperature measurements in the energy storage system were determined by means of the data logger at 10 seconds intervals and recorded in the computer via the RS232 interface.

The solidified ice amount is essential for the calculation of the latent energy storage was obtained by measuring the mean ice diameter on each pipe for one hour intervals. The electrical power demanded from the chiller was also recorded by the counter at one hour intervals. Experimental results, consisting of inlet and outlet temperature of the secondary fluid, ice diameter and electrical energy, are listed Table 2.3, for four different secondary flow rates.

Table 2.2 Calibration values of the thermocouple wires

$Y = Ax + B$			
Y: Actual Value (˚C)		*x: Indicated value (˚C)*	
Thermocouple wire Number	**A**	**B**	**R^2**
101	1.0220	1.9278	0.9981
102	1.0193	1.9260	0.9977
103	1.0166	1.7088	0.9981
104	1.0175	1.8214	0.9973
105	1.0221	1.4768	0.9972
106	1.0292	1.6232	0.9966
107	1.0209	1.6717	0.9972
108	1.0183	1.7367	0.9971
109	1.0161	2.0303	0.9974
110	1.0159	2.0760	0.9972
111	1.0101	1.8901	0.9973
112	1.0226	1.8333	0.9964
113	1.0074	2.0218	0.9973
114	1.0187	1.9834	0.9963
115	1.0122	2.0602	0.9975
116	1.0106	2.1735	0.9976
117	1.0266	2.1159	0.9972
118	1.0184	2.2470	0.9976
119	1.0120	2.3504	0.9978
120	1.0089	2.5065	0.9970

Table 2.3 Experimental data for each flow rate during the energy storage

a) Volumetric Flow Rate: 20 l/min

Time	Measured Temperatures		Avg. Ice Diameter	Electrical demand
	T_{inlet}	T_{outlet}		
(Hour)	(˚C)	(˚C)	(mm)	(kWh)
1	-7.1	-4.1	0.0	2.5
2	-7.7	-4.6	21.9	2.4
3	-8.3	-4.8	28.7	2.5
4	-8.4	-5.0	36.8	2.5
5	-8.5	-5.2	40.6	2.5
6	-8.6	-5.3	43.7	2.5
7	-8.6	-5.4	47.3	2.6
8	-8.6	-5.4	50.5	2.5
9	-8.6	-5.5	53.0	2.5
10	-8.6	-5.5	56.1	2.5
11	-8.6	-5.5	58.5	2.4
12	-8.6	-5.5	60.4	2.4

b) Volumetric Flow Rate: 30 l/min

Time	Measured Temperatures		Avg. Ice Diameter	Electrical demand
	T_{inlet}	T_{outlet}		
(Hour)	(˚C)	(˚C)	(mm)	(kWh)
1	-8.6	-6.1	0.0	2.4
2	-8.7	-6.1	27.2	2.5
3	-8.8	-6.4	35.2	2.2
4	-9.0	-6.7	41.1	2.3
5	-9.2	-6.9	45.1	2.3
6	-8.4	-6.3	49.1	2.4
7	-8.4	-6.4	52.7	2.5
8	-8.4	-6.4	55.7	2.4
9	-8.4	-6.5	58.2	2.3
10	-8.4	-6.5	61.0	2.3
11	-8.5	-6.6	63.5	2.4
12	-8.5	-6.6	66.1	2.4

c) Volumetric Flow Rate: 40 l/min

Time	Measured Temperatures		Avg. Ice Diameter	Electrical demand
	T_{inlet}	T_{outlet}		
(Hour)	(˚C)	(˚C)	(mm)	(kWh)
1	-7.7	-5.7	0.0	2.4
2	-7.5	-5.5	31.4	2.4
3	-7.8	-5.9	36.7	2.3
4	-8.1	-6.2	42.3	2.5
5	-8.1	-6.3	47.1	2.5
6	-8.1	-6.3	51.1	2.5
7	-8.1	-6.3	54.8	2.5
8	-8.1	-6.4	57.9	2.5
9	-8.1	-6.4	60.9	2.5
10	-8.2	-6.5	63.6	2.5
11	-8.2	-6.5	66.2	2.5
12	-8.3	-6.6	68.2	2.5

d) Volumetric Flow Rate: 50 l/min

Time	Measured Temperatures		Avg. Ice Diameter	Electrical demand
	T_{inlet}	T_{outlet}		
(Hour)	(˚C)	(˚C)	(mm)	(kWh)
1	-6.5	-5.3	19.0	2.5
2	-6.1	-5.0	27.9	2.4
3	-6.3	-5.3	34.8	2.5
4	-6.5	-5.5	40.5	2.5
5	-6.8	-5.8	44.7	2.5
6	-7.0	-6.0	49.0	2.5
7	-7.1	-6.1	52.6	2.6
8	-7.0	-6.1	56.0	2.6
9	-7.0	-6.1	58.7	2.5
10	-7.1	-6.2	61.9	2.6
11	-7.1	-6.2	64.3	2.6
12	-7.2	-6.3	67.0	2.6

2.2.2 Uncertainty Analysis

Experimental studies, naturally, cause some uncertainties and unpredictable errors. Such diversions may arise due to human nature reading errors, instrumental manufacturing errors, environmental condition effects or calibration errors and all of which can not be taken into account for evaluating the experimental results. Recently many studies were performed about the uncertainty theory, to investigate the accuracy of the estimations for experiments, experimental setup and instruments (Asan and Namli, 1997; Hepbasli and Akdemir, 2004). In these researches,

computation of the experimental results mainly depend upon inlet, outlet and surface temperatures, volumetric flow rate of the secondary coolant, thermo-physical properties of the materials and geometric dimensions of the test section. Latent energy is the dominant one, in comparison with the sensible energy, for calculating the total stored energy and total uncertainty for computing the latent energy can be obtained as ±3.0 %, from the uncertainties of above-mentioned parameters that are given in Table 2.4 via Holman (2001) methodology,

2.2.2.1 Temperature Measurement Errors

Temperature measurement errors include following uncertainties and total uncertainties for inlet, outlet and surface temperatures are given in Table 2.4

Uncertainties arise from,

Thermocouples	:	±1.0 %
Reference temperature	:	±1.0 %
Data logger system	:	±0.3 %
Connections	:	±0.1 %
Inlet temperature measurement	:	±0.5 %
Outlet temperature measurement	:	±2-3 %
Surface temperature measurement	:	±0.5-1.0 %

2.2.2.2 Volumetric Flow Rate Measurement Errors

Volumetric flow rate measurement errors include following uncertainties and total uncertainty for flow rate is given in Table 2.4,

Uncertainties arise from,

Flow meter reading	:	±1.0-1.5 %
System leakages	:	±2.0-3.0 %
Temperature difference (*Density difference*)	:	±0.5-1.0 %

2.2.2.3 Other Errors

Uncertainties arise from manufacturing errors and selecting the thermo-physical properties for materials can be listed as follows,

Uncertainties arise from,

Pipe diameter differences	:	±1.0%
Pipe length differences	:	±2.0-3.0 %
Thermo-physical properties selection	:	±0.5-1.0 %

Table 2.4 Total uncertainties for measured and experimental parameters

Parameter	**Nominal Value**	**Unit**	**Total Uncertainty (%)**
Inlet temperature of the secondary coolant	-6.0 – -10.0	˚C	±1.265
Outlet temperature of the secondary coolant	-4.0 – -7.0	˚C	±2.313
Surface temperature of the pipe	-2.0 – -8.0	˚C	±1.383
Volumetric flow rate of the secondary coolant	20 – 60	l/min	±2.646
Polyethylene pipe diameter (D)	17	mm	±1
Polyethylene pipe length (L)	13	m	±1.5
Ice thickness measurement	20 – 70	mm	±0.1
Thermo-physical properties of the materials (ρ, v, k, c_p…)	-	-	±0.15

2.2.3 Experimental Procedure

In all experiments, the initial temperature of the phase change material (water) was taken a little higher than the fusion temperature, so that the natural convection effects inside the water can be neglected. In order to achieve this, the chiller, which is integrated to the system, was operated before starting the experiments. The secondary fluid flowing through the evaporator dropped the temperature of the water in the storage tank down to the desired level. The experiments were started when the temperature of the system was near 1ºC. In that condition no ice formation was observed on the surface of the pipes.

Four charge tests were performed. Each test required an average of 12 hours. During the experiments, the secondary fluid was circulated through the evaporator where it was cooled below the phase change temperature of the water, before entering the energy storage tank. The required secondary fluid flow rate was kept constant during each test by controlling the desired value of flow rate at the acrylic tube flow meter.

2.3 Determination of The Total Stored Energy

Energy transferred from the ethylene-glycol to the tank, consists of three components of the energy: *latent energy* that occurs from the solidification of water into ice, *sensible energy* that appears on the temperature drop of both ice and water and *gained energy* which is the heat gain from the surroundings of the storage tank. The total energy stored and the energy transmitted from the secondary coolant can be written as follows,

$$Q_{stored} = Q_{latent} + Q_{sensible,ice} + Q_{sensible,water} \tag{2.1}$$

$$Q_{total} = Q_{stored} + Q_{gain} \tag{2.2}$$

2.3.1 Latent Energy

In order to be able to calculate the latent thermal energy stored in the thermal energy storage system, it is essential to find the amount of ice inside the tank. The latent energy is defined as,

$$Q_{latent} = m_{ice}\Delta H \tag{2.3}$$

Here, m_{ice} represents the ice amount that solidified around pipes and calculated from the ice thickness. The methods that are commonly used to measure the ice thickness (Shi et al., 2005) in an ice storage system are, (a) water level measurement based on the volume expansion; (b) mechanical ice layer thickness measurement; (c) measurement utilizing the conductivity difference of ice and water; (d) freezing temperature measurement according to the temperature difference between water and refrigerant or glycol in the pipe and (e) other methods. Since method (b) is the most suitable method in a closed system, the volume of ice formed at each time step was obtained via measuring the average diameter of ice around all pipes.

The total volume of ice, formed around pipes at each time step, were calculated by using the formula below,

$$V_{ice}(t) = \sum_{i=1}^{8} \frac{\pi}{4}\left(D_{ice}^2(t) - D_o^2\right)L \tag{2.4}$$

The latent energy stored in the energy storage system is calculated by the amount of ice formed around the pipe at each time step. So it was calculated by using the following equation,

$$Q_{lat}(t) = \rho_{ice} V_{ice} \Delta H \tag{2.5}$$

2.3.2 Sensible Energy

The amount of the sensible energy, both stored in the volumes of ice and water in the energy storing system at each time step is calculated as follows,

$$Q_{sen}(t) = \left\{m_{water,i} c_{water} \overline{T}_{water,i}\right\} - \left\{m_{ice} c_{ice} \overline{T}_{ice}(t) + \left[m_{water,i} - m_{ice}(t)\right] c_{water} \overline{T}_{water}(t)\right\} \tag{2.6}$$

Here, $\overline{T}_{ice}(t)$ is the average temperature of the ice which is calculated by assuming that the distribution of the temperature inside the ice changes logarithmically. While computing $\overline{T}_{ice}(t)$, the mean values of the pipe surface temperatures are measured and taken as the pipe surface temperature, as shown in Figure 2.4.

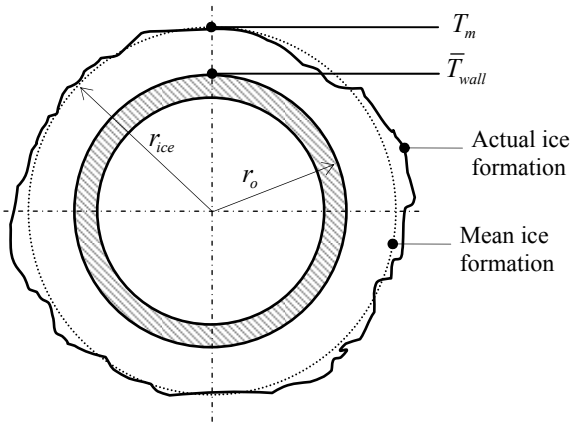

Figure 2.4 Solidification around pipe

For the radial coordinate systems, the temperature distribution through *r-axis* can be derived from widely known "*the heat conduction equation*",

$$\frac{1}{r}\frac{\partial}{\partial r}\left(kr\frac{\partial T}{\partial r}\right)=0 \tag{2.7}$$

General solution of the differential equation can be written with the boundary conditions, as follows,

$$T(r)=C_1\ln r+C_2$$

Boundary conditions: $r=r_{wall} \rightarrow T=\overline{T}_{wall}$

$r=r_{ice} \rightarrow T=T_m$

Thus, the temperature distribution of such a cylindrical system can be written as,

$$T(r)=\frac{T_{wall}-T_m}{\ln(r_{wall}/r_{ice})}\ln(r/r_{ice})+T_m \tag{2.8}$$

$\overline{T}_{ice}(t)$ can be obtained with the integration of the Equation (2.8) through solidification front, as follows;

$$\overline{T}_{ice}(t)=\frac{2}{\left(r_{ice}^2-r_{wall}^2\right)}\overline{T}_{wall}\int_{r_{wall}}^{r_{ice}}\left[\frac{1}{\ln\left(r_{wall}/r_{ice}\right)}\ln\left(r/r_{ice}\right)+T_m\right]rdr \tag{2.9}$$

Here, the temperatures of $\overline{T}_{water}(t)$ and $\overline{T}_{water,i}$ are taken as the mean value of the water temperature measured by thermocouples at two different locations in the tank, for $t>0$ and $t=0$, respectively.

2.3.3 Gained Energy

Heat gain from sorroundings of the tank is calculated by using *Fourier Law*, which is defined as,

$$q_{gain}=-A_{tank}\frac{dT}{R''_{total}} \tag{2.10}$$

Here, the total heat transfer area of the tank is $A_{tank}\,(=8.353m^2)$ and the total thermal resistance of the tank wall (R''_{total}) is obtained for the cross-section of the tank wall, which is represented in the Figure 2.5.

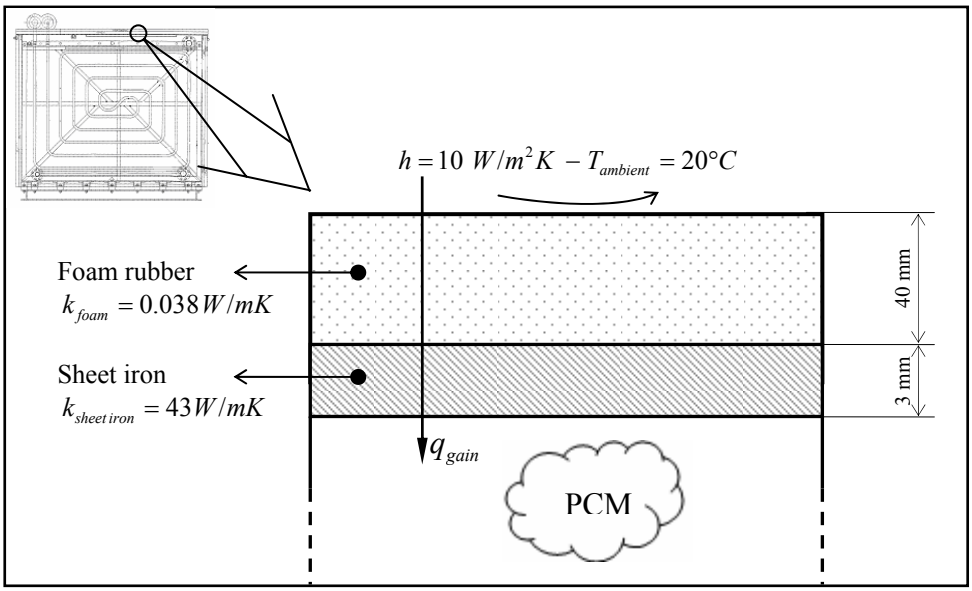

Figure 2.5 Cross-section of the tank wall

$$q_{gain} = -8.353 \frac{(0-20)}{\frac{3\times10^{-3}}{43} + \frac{40\times10^{-3}}{0.038} + \frac{1}{10}} \tag{2.11}$$

$$q_{gain} = 151.87W \tag{2.12}$$

The total heat gain form the tank surface, along a period of time (t) can be written as,

$$Q_{gain} = 151.87 \times t \tag{2.13}$$

2.4 Experimental Results

In this study, the effect of various inlet conditions of the secondary fluid flow rate and temperature on thermal energy storage in ice-on-coil thermal energy storage system for charging process is investigated experimentally and numerically. Hence, to observe this variation, experiments were repeated for four different volumetric flow rates (20, 30, 40 and 50 l/min). In each experiment, charging time was set to 12 hours and during this period, the electrical energy retreated by chiller and sensible, latent and total energies stored in the tank were calculated as above mentioned methodology. These results for each volumetric flow rates are given in Table 2.5.

According to the Table 2.5, total stored energy rises with increasing the volumetric flow rate from 20 l/min through 40 l/min. Meanwhile, it should not be expected that the stored energy always increase with the increasing flow rate, as seen from the data in Table 2.5; from 40 l/min to 50 l/min, stored energy decreases, since the cooling capacity of the chiller is limited, so the inlet temperature of the coolant rise with the increasing flow rate. This effect can also be seen in Figure 2.6, where the experimental results are given with the bulk inlet temperatures.

Table 2.5 Latent, sensible and total energy stored in system

(Coolant flow rates: a. 20 l/min, b. 30 l/min, c. 40 l/min, d. 50 l/min)

a) Volumetric Flow Rate: 20 l/min

Time	Q_{latent}	$Q_{sensible}$	Q_{gain}	Q_{total}
(Hour)	(kJ)	(kJ)	(kJ)	(kJ)
1	0.0	7308.9	546.7	7855.6
2	4866.6	12153.1	1093.5	18113.1
3	13460.4	12427.4	1640.2	27528.0
4	24602.5	12337.5	2186.9	39126.9
5	32221.0	12656.3	2733.7	47610.9
6	40732.9	12240.5	3280.4	56253.8
7	48958.5	12167.6	3827.1	64953.2
8	56663.0	12045.7	4373.9	73082.5
9	63322.4	11867.0	4920.6	80109.9
10	71724.6	11489.5	5467.3	88681.5
11	78682.6	11428.6	6014.1	96125.2
12	84240.2	11059.4	6560.8	101860.3

b) Volumetric Flow Rate: 30 l/min

Time	Q_{latent}	$Q_{sensible}$	Q_{gain}	Q_{total}
(Hour)	(kJ)	(kJ)	(kJ)	(kJ)
1	0.0	9400.8	546.7	9947.6
2	11325.4	10803.0	1093.5	23221.8
3	23747.8	11507.4	1640.2	36895.3
4	35078.5	11855.1	2186.9	49120.5
5	43727.2	12007.4	2733.7	58468.3
6	53153.0	11624.0	3280.4	68057.5
7	62363.7	11508.8	3827.1	77699.6
8	70479.9	11367.8	4373.9	86221.6
9	77722.4	11463.2	4920.6	94106.2
10	85932.8	10970.8	5467.3	102370.9
11	93849.6	11040.6	6014.1	110904.2
12	102043.0	10652.3	6560.8	119256.1

c) Volumetric Flow Rate: 40 l/min

Time	Q_{latent}	$Q_{sensible}$	Q_{gain}	Q_{total}
(Hour)	(kJ)	(kJ)	(kJ)	(kJ)
1	0.0	5720.0	546.7	6266.7
2	17412.1	7613.6	1093.5	26119.2
3	26555.6	8633.6	1640.2	36829.4
4	37484.3	9012.2	2186.9	48683.4
5	48309.8	8760.6	2733.7	59804.0
6	58081.6	8468.5	3280.4	69830.5
7	67887.7	8377.7	3827.1	80092.6
8	76780.8	8443.4	4373.9	89598.1
9	85523.3	8252.0	4920.6	98695.9
10	94076.0	8200.9	5467.3	107744.2
11	102467.3	8103.9	6014.1	116585.2
12	109312.4	8208.6	6560.8	124081.8

d) Volumetric Flow Rate: 50 l/min

Time	Q_{latent}	$Q_{sensible}$	Q_{gain}	Q_{total}
(Hour)	(kJ)	(kJ)	(kJ)	(kJ)
1	1863.5	7663.7	546.7	10073.9
2	12280.0	10088.4	1093.5	23461.9
3	23017.8	11063.8	1640.2	35721.8
4	33852.8	11674.8	2186.9	47714.4
5	42914.1	11835.5	2733.7	57483.3
6	52832.3	11736.5	3280.4	67849.2
7	62004.2	11594.8	3827.1	77426.1
8	71216.5	11208.7	4373.9	86799.1
9	79153.0	10900.5	4920.6	94974.1
10	88709.2	10678.9	5467.3	104855.5
11	96456.5	10701.5	6014.1	113172.0
12	105132.9	10460.7	6560.8	122154.4

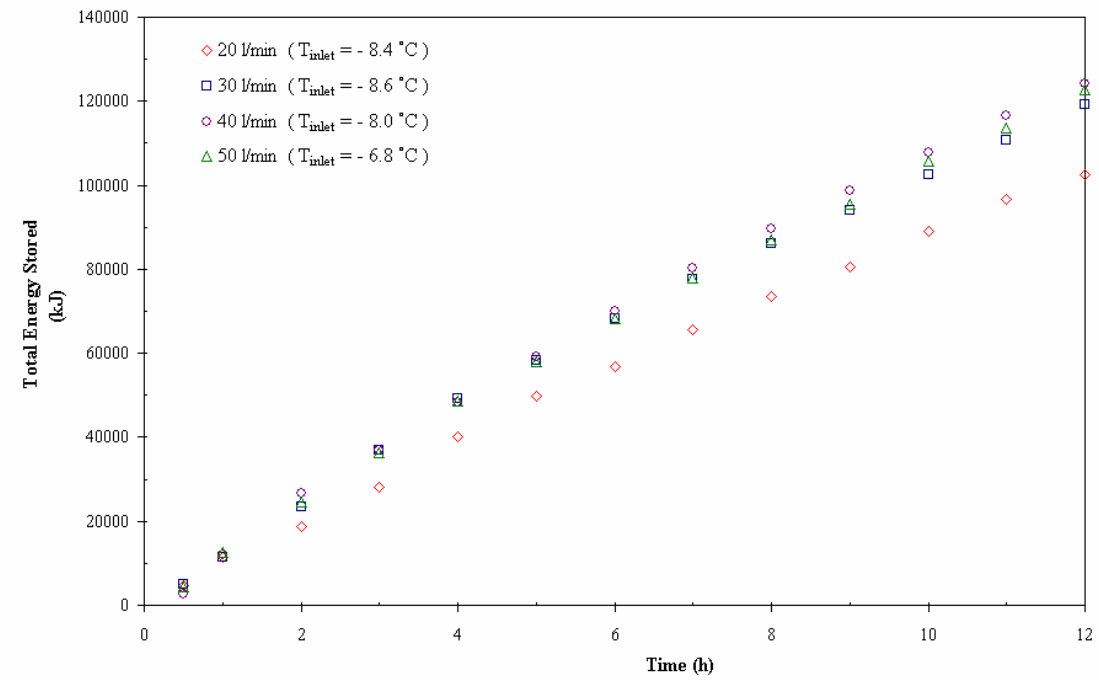

Figure 2.6 Experimental energy storage through 12 hours, for four volumetric flow rates with inlet bulk temperature

CHAPTER THREE
MATHEMATICAL FORMULATION AND NUMERICAL MODEL

3.1 Introduction

In the latent energy storage system, the secondary coolant (brine) flows inside eight polyethylene pipes and cool energy is stored inside the ice storage tank via making ice around the pipes. Since the numerical analysis of such a three dimensional and time dependent system is difficult to be modeled, it is sufficient to simplify the system by using symmetry surfaces and analyzing only 1/8 part of the physical system, as shown in Figure 3.1.

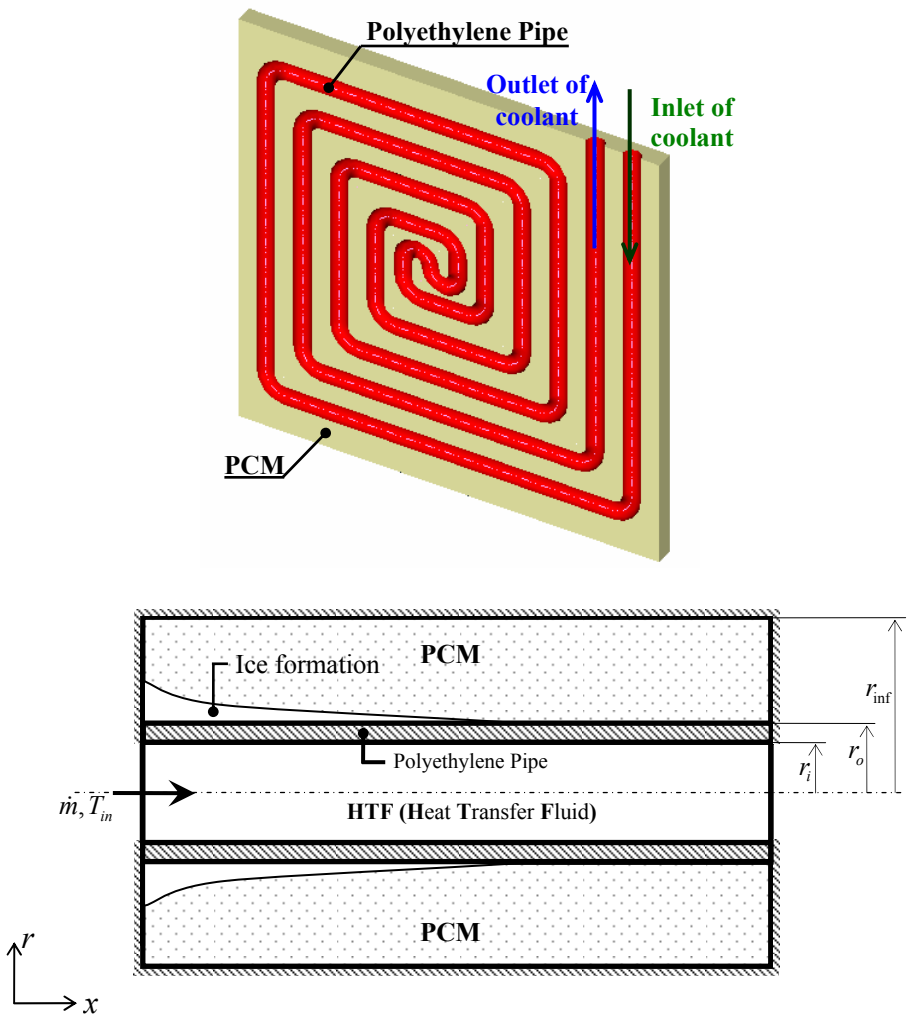

Figure 3.1 Physical model and mathematical model

A schematic representation of the numerical model for an energy storage unit is shown in Figure 3.1. The PCM fills the annular space around the pipe, with inner radius r_o and outer radius $r_{\inf}$, while the heat transfer fluid flows inside the pipe. The pipe wall has inside and outside radii of r_i and r_o respectively. The outside wall of the energy storage unit is insulated. The thermo-physical properties of the PCM, pipe wall and heat transfer fluid are independent of temperature, but the properties of the PCM can be different for the solid and liquid phases. Initially, the system is at a temperature of T_i higher than T_m. Suddenly, HTF having the temperature of T_{in} which is lower than T_m, flows in the pipe and solidification occurs around the pipe. Formulating a mathematical model to represent this physical system, the system is divided into the following three subsections;

1. Tube flow of heat transfer fluid,
2. The pipe wall,
3. The region filled by the phase change material.

3.2 Governing Equations

Governing equations for the solution domain can be gained via energy balance for arbitrary control volume for each subsection. The first law of the thermodynamics determines the energy balance as follows,

$$\dot{E}_{inlet} + \dot{E}_{generation} = \dot{E}_{outlet} + \dot{E}_{stored} \tag{3.1}$$

3.2.1 Equations For Heat Transfer Fluid

For an internal flow, hydro-dynamically fully developed, energy balance for a differential control volume, as seen in Figure 3.2, can be written as in the Equation (3.1) with the components of,

$$\dot{E}_{generation} = 0 \tag{3.2}$$

$$\dot{E}_{inlet} = q_{conv} + q_{cond} \text{ or } \dot{E}_{inlet} = \dot{m}c_f T^0 + q_x \tag{3.3}$$

$$\dot{E}_{outlet} = q_{conv} + q_{cond} \text{ or } \dot{E}_{outlet} = \dot{m}c_f T^0_{x+dx} + hA_l\left(T^0 - T^0_{x+dx}\right) + q_{x+dx} \tag{3.4}$$

$$\dot{E}_{stored} = \rho c_f A dx \frac{\partial T}{\partial t} \text{ or } \dot{E}_{stored} = (\rho c)_f A dx \frac{\partial T^0}{\partial t} \tag{3.5}$$

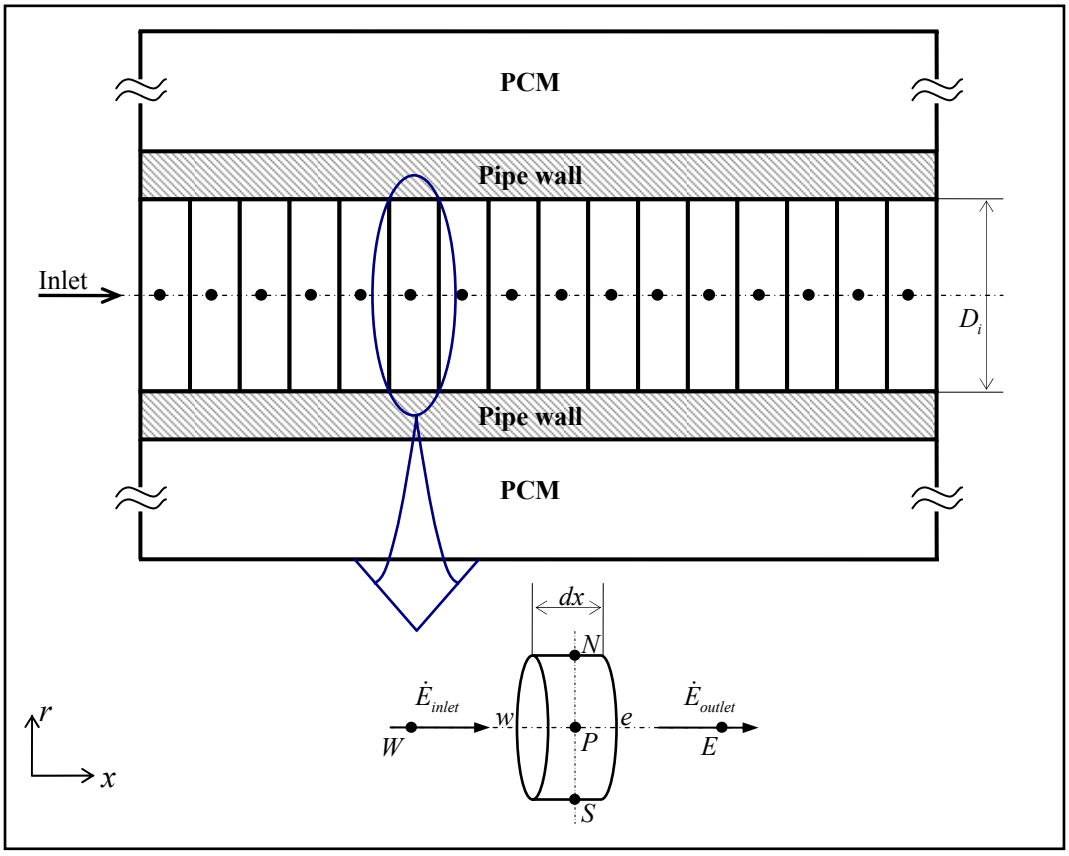

Figure 3.2 Energy balance for the heat transfer fluid

where,

$$q_x = -k_w A \frac{\partial T^0}{\partial x} \text{ and } q_{x+dx} = q_x + \frac{\partial q_x}{\partial x} dx \tag{3.6}$$

here, $A\,(=\pi r_i^2)$ is the cross section and $A_l\,(=2\pi r_i dx)$ is the lateral area of the control volume. Equations (3.2) to (3.6) can be substituted in Equation (3.1),

$$\dot{m}c_f T^0 + q_x = \dot{m}c_f T^0_{x+dx} + hA_l\left(T^0 - T^0_{x+dx}\right) + q_{x+dx} + (\rho c)_f A dx \frac{\partial T^0}{\partial t} \tag{3.7}$$

where, it is assumed that fully developed conditions exist at the pipe inlet, so the mass flow rate of the fluid is defined as, $\dot{m} = \rho_f A u_m$.

Hence Equation (3.7) can be re-arranged as follows,

$$-\rho_f\left(\pi r_i^2\right)u_m c_f\left(T^0_{x+dx} - T^0_x\right) - h\left(2\pi r_i dx\right)\left(T^0 - T^0_w\right) = (\rho c)_f\left(\pi r_i^2\right)dx\frac{\partial T^0}{\partial t} - \frac{\partial}{\partial x}\left(k_w \pi r_i^2 \frac{\partial T^0}{\partial x}\right)dx \tag{3.8}$$

Assuming that the temperature is constant through radial direction and axial conduction is negligible, the equation can be simplified,

$$-(\rho c)_f u_m \frac{\partial T^0}{\partial x} + \frac{4h}{D_i}\left(T^0_w - T^0\right) = (\rho c)_f \frac{\partial T^0}{\partial t} \tag{3.9}$$

As a result, energy equation for the heat transfer fluid can be expressed as;

$$(\rho c)_f \frac{\partial T^0}{\partial t} = \frac{4h}{D_i}\left(T^0_w - T^0\right) - (\rho c)_f u_m \frac{\partial T^0}{\partial x} \tag{3.10}$$

3.2.2 Equations For The Pipe Wall

For the pipe wall, two-dimensional heat conduction equation obtained from the heat balance of a differential element, as seen in Figure 3.3. The components of the Equation (3.1) can be written as,

$$\dot{E}_{generation} = 0 \tag{3.11}$$

$$\dot{E}_{inlet} = q_x + q_r \tag{3.12}$$

$$\dot{E}_{outlet} = q_{x+dx} + q_{r+dr} \tag{3.13}$$

$$\dot{E}_{stored} = (\rho c)_w A dx \frac{\partial T^0}{\partial t} \tag{3.14}$$

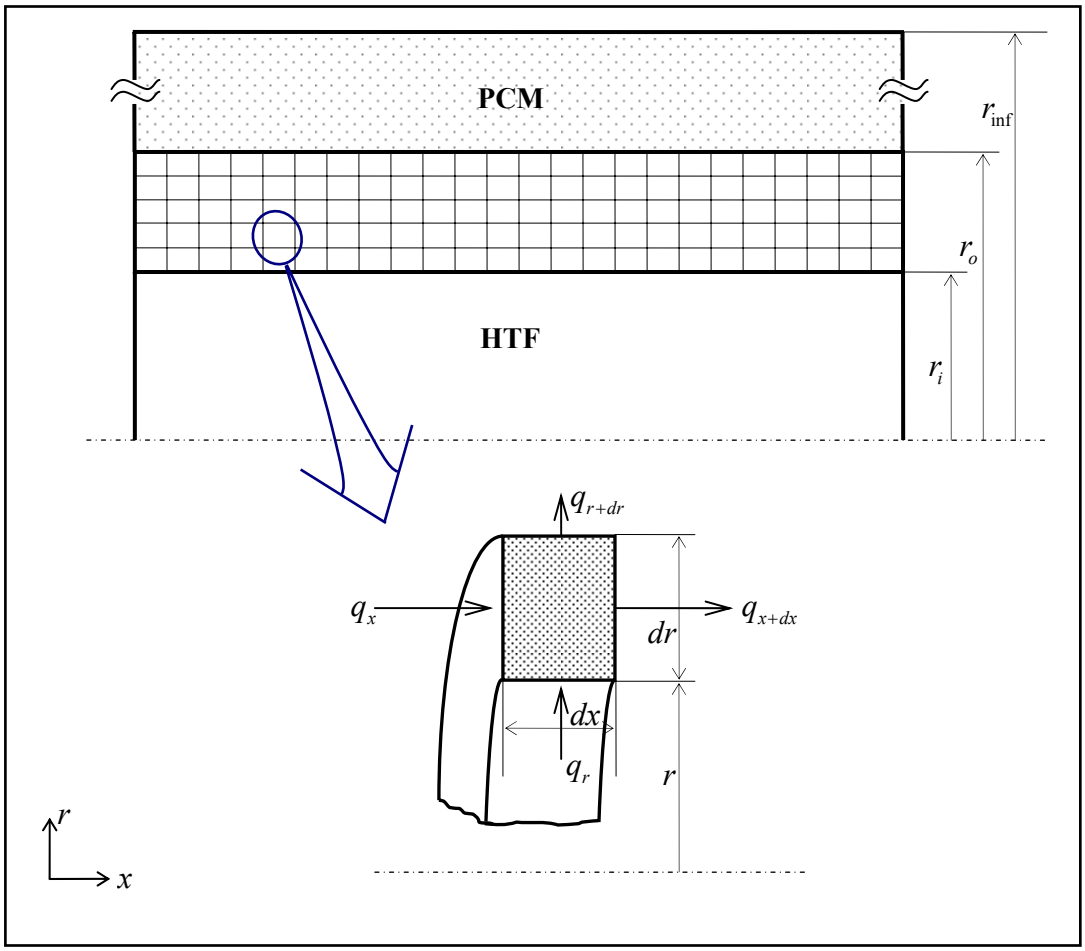

Figure 3.3 Energy balance for the pipe wall

where,

$$q_x = -k_w A \frac{\partial T^0}{\partial x} \text{ and } q_{x+dx} = q_x + \frac{\partial q_x}{\partial x} dx \tag{3.15}$$

$$q_r = -k_w A_l \frac{\partial T^0}{\partial r} \text{ and } q_{r+dr} = q_r + \frac{\partial q_r}{\partial r} dr \tag{3.16}$$

Thus, energy balance in Equation (3.1), can be written as,

$$\left(q_x + q_r\right) - \left(q_{x+dx} + q_{r+dr}\right) = \left(\rho c\right)_w \left(2\pi r dr dx\right)\frac{\partial T^0}{\partial t} \tag{3.17}$$

$$\frac{\partial}{\partial x}\left(k_w 2\pi r dr \frac{\partial T^0}{\partial x}\right)dx + \frac{\partial}{\partial r}\left(k_w 2\pi r dx \frac{\partial T^0}{\partial r}\right)dr = \left(\rho c\right)_w \left(2\pi r dr dx\right)\frac{\partial T^0}{\partial t} \tag{3.18}$$

Hence energy equation for the pipe wall can be expressed as,

$$\left(\rho c\right)_w \frac{\partial T^0}{\partial t} = \frac{\partial}{\partial x}\left(k_w \frac{\partial T^0}{\partial x}\right) + \frac{1}{r}\frac{\partial}{\partial r}\left(k_w r \frac{\partial T^0}{\partial r}\right) \tag{3.19}$$

3.2.3 Equations For Phase Change Material (PCM)

As the initial temperature of the system is considered to be the same or close to the phase change temperature, the natural convection effect around the pipe can be neglected. The heat conduction in the PCM is described by a temperature transforming method using a fixed grid numerical model (Cao and Faghri, 1990). This model assumes that solidification process occurs over a range of phase change temperature from $T_m - \delta T_m$ to $T_m + \delta T_m$, but it can also be successfully used to simulate the solidification process occurring at a single temperature by taking a small range of phase change temperature, $2\delta T_m$. The governing equation for PCM (water) can be obtained as,

$$\frac{\partial H}{\partial t} = \left[\frac{1}{r}\frac{\partial}{\partial r}\left(kr\frac{\partial T}{\partial r}\right) + \frac{\partial}{\partial x}\left(k\frac{\partial T}{\partial x}\right)\right] \tag{3.20}$$

The mathematical model is constituted under following assumptions,

1. The thermo-physical properties of the PCM are all constant with respect to temperature, but the properties can be different in the solid and liquid phases.
2. The PCM is homogeneous and isotropic.
3. The effect of natural convection in the liquid PCM is ignored.

The specific enthalpy of the material is computed as the sum of the sensible enthalpy, h, and the latent heat, ΔH;

$$H = h + \rho \Delta H f \tag{3.21}$$

where, f is the liquid fraction and h can be defined as,

$$\frac{dh}{dT} = c_p \tag{3.22}$$

so the sensible enthalpy can be derived as,

$$h = h_{ref} + \int_{T_{ref}}^{T} \rho c_p dT \tag{3.23}$$

The $H - T$ curve for the PCM used (water) is drawn in Figure 3.4, and it is shown that, the specific enthalpy H, *the enthalpy per unit volume*, is related to the temperature field and the relationship during phase change is assumed to be linear. Specific enthalpy of the PCM in its solid state, at the temperature of, $T_m - \delta T_m$, is zero ($H_s = 0$).

For each phase, the relation between enthalpy and temperature can be derived from the Equations (3.21) and (3.23);

Solid phase, $(T < T_m - \delta T_m)$

$$H(T) = \left(\rho c_p\right)_s \left(T - T_m + \delta T_m\right) \tag{3.24}$$

Mushy phase, $(T_m - \delta T_m < T < T_m + \delta T_m)$

$$H(T) = \left(\rho c_p\right)_m \left(T - T_m\right) + \rho \frac{\Delta H}{2\delta T_m} \left(T - T_m\right) + \left(\rho c_p\right)_m \delta T_m + \rho \frac{\Delta H}{2} \tag{3.25}$$

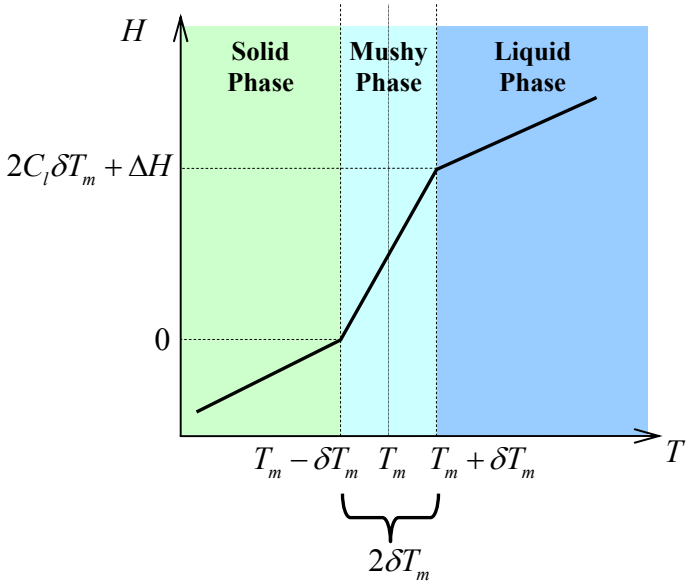

Figure 3.4 Enthalpy - temperature relationship

Liquid phase, $(T > T_m + \delta T_m)$

$$H(T) = \left(\rho c_p\right)_l \left(T - T_m + \delta T_m\right) + \rho \Delta H \tag{3.26}$$

Simplifying the equations, temperature can be written as $T^* = T - T_m$ and, the $H - T$ relations for three regions are,

$$H(T) = \begin{cases} C_s T^* + C_s \delta T_m & T^* < -\delta T_m \\ \left(C_m + \rho \dfrac{\Delta H}{2\delta T_m} \right) T^* + C_m \delta T_m + \rho \dfrac{\Delta H}{2} & -\delta T_m \le T^* \le \delta T_m \\ C_l T^* + C_l \delta T_m + \rho \Delta H & T^* > \delta T_m \end{cases} \tag{3.27}$$

Here, C_s, C_l and C_m represent the heat capacities of *solid phase*, *liquid phase* and *mushy phase* respectively where the heat capacity is defined as,

$$C = c_p \rho \tag{3.28}$$

and for mushy zone, C_m is the average of the two main phases,

$$C_m = \frac{C_l + C_s}{2} \tag{3.29}$$

Enthalpy can be expressed in linear form, from the integration of Equation (3.22);

$$H = CT + S \tag{3.30}$$

where, S is known as the source term. Here the heat capacity and the source terms are determined from Equation (3.27), as follows;

$$C(T) = \begin{cases} C_s & T^* < -\delta T_m \quad \text{Solid Phase} \\ C_m + \rho \dfrac{\Delta H}{2\delta T_m} & -\delta T_m \le T^* \le \delta T_m \quad \text{Mushy Phase} \\ C_l & T^* > \delta T_m \quad \text{Liquid Phase} \end{cases} \tag{3.31}$$

$$S(T) = \begin{cases} C_s \delta T_m & T^* < -\delta T_m \quad \text{Solid Phase} \\ C_m \delta T_m + \rho \dfrac{\Delta H}{2} & -\delta T_m \le T^* \le \delta T_m \quad \text{Mushy Phase} \\ C_l \delta T_m + \rho \Delta H & T^* > \delta T_m \quad \text{Liquid Phase} \end{cases} \tag{3.32}$$

As the thermo-physical properties of the PCM, C and S terms are also different for each solid, mushy and liquid phases, but they are constant for arbitrary phase, as illustrated in Figure 3.5.

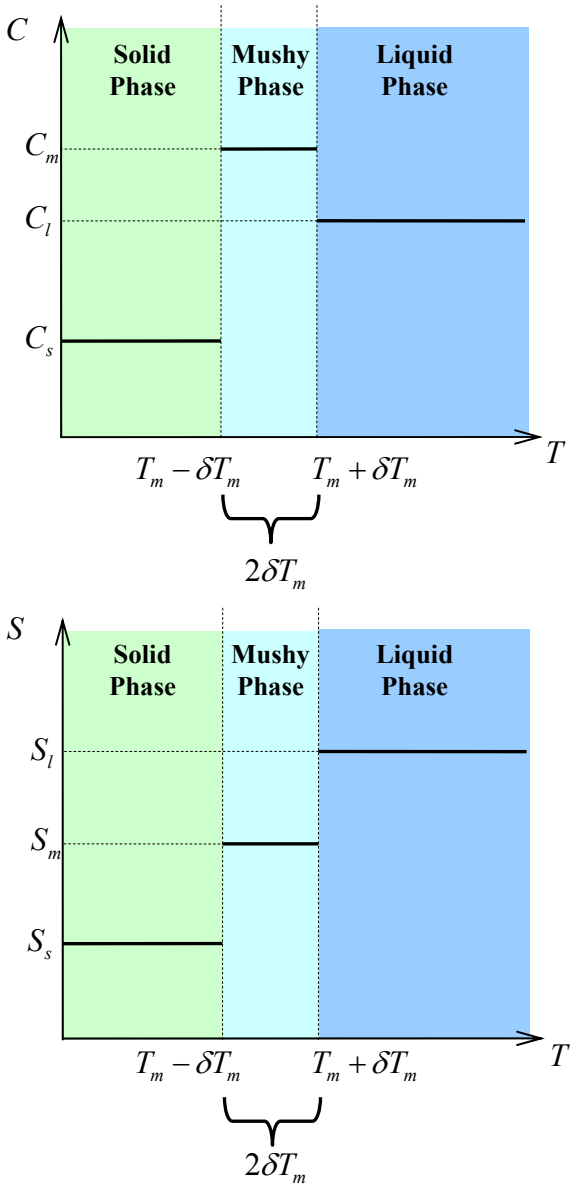

Figure 3.5 Heat capacity and source term relationship with temperature

3.3 Non-dimensional Form of Governing Equations

Governing equations could be written in non-dimensional form, to reduce the number of parameters, thus the solution algorithm becomes simpler than the dimensional form. All equations are transformed into non-dimensional form, and the dimensionless variables and groups are first introduced as in Table 3.1.

Table 3.1 Dimensionless variables

	Dimensional form	Dimensionless form
Co-ordinate along radial direction	r	$R = \frac{r}{D_i}$
Co-ordinate along axial direction	x	$X = \frac{r}{D_i}$
Time	t	$\tau = \frac{\alpha_f t}{D_i^2}$
Temperature	T	$\theta = \frac{T - T_m}{T_m - T_{in}}$
Phase change temperature range	δT_m	$\delta\theta_m = \frac{\delta T_m}{(T_m - T_{in})}$
Thermal conductivity	k	$K = \frac{k}{k_l}$
Thermal diffusivity	α	$\alpha = \frac{k}{\rho c}$
Heat capacity	$C^0 (= \rho c)$	$C = \frac{C^0}{\rho_l c_l}$
Source term	S^0	$S = \frac{S^0}{\rho_l c_l (T_m - T_{in})}$
Reynolds number	-	$\mathrm{Re}_f = \frac{4\dot{m}}{\pi D \mu_f}$
Prandtl number	-	$\mathrm{Pr}_f = \frac{\nu_f}{\alpha_f}$
Stefan number	-	$Ste = \frac{c_l (T_m - T_{in})}{\Delta H}$
Peclet number	-	$\mathrm{Pe}_f = \mathrm{Re}_f \mathrm{Pr}_f$

3.3.1 Non-dimensional Form of HTF Equation

Governing equation for the heat transfer fluid is obtained as in Equation (3.10) and non-dimensional form of this equation can be obtained as follows, using the parameters listed in Table 3.1;

$$\rho_f \frac{c_f \alpha_f}{D_i^2} \frac{\partial\theta}{\partial\tau} = \frac{4h}{D_i}(\theta_w - \theta_f) - \rho_f \frac{c_f u_m}{D_i} \frac{\partial\theta}{\partial X} \tag{3.33}$$

$$\frac{\partial\theta}{\partial\tau} = 4Nu(\theta_w - \theta_f) - \frac{\mu_f c_f}{k_f} \rho_f \frac{u_m D_i}{\mu_f} \frac{\partial\theta}{\partial X} \tag{3.34}$$

Energy equation of the heat transfer fluid can be expressed in dimensionless form,

$$\frac{\partial\theta}{\partial\tau} = 4Nu\left(\theta_w - \theta_f\right) - \mathrm{PrRe}\frac{\partial\theta}{\partial X} \tag{3.35}$$

Here, for laminar and hydro-dynamically fully developed flow, Nusselt number is obtained from analytic method, developed by Kays and Crawford (1980) and Zhang and Faghri (1996),

$$\left(Nu\right)_j = \frac{\sum_{k=1}^{j}\Delta\theta_k\sum_{n=0}^{\infty}G_n\exp\left[-\frac{2\lambda_n^2}{Pe_f}\left(X-\left(k-1\right)\Delta X\right)\right]}{2\sum_{k=1}^{j}\Delta\theta_k\sum_{n=0}^{\infty}\frac{G_n}{\lambda_n^2}\exp\left[-\frac{2\lambda_n^2}{Pe_f}\left(X-\left(k-1\right)\Delta X\right)\right]} \tag{3.36}$$

where,

$$\Delta\theta_k = \left(\theta_{Ri}\right)_k - \left(\theta_{Ri}\right)_{k-1} \text{ and } j = \mathrm{int}\left(\frac{X}{\Delta X}\right)+1 \tag{3.37}$$

The eigenvalues λ_n and the constants G_n in Equation (3.36) are given in Table 3.2. For turbulent flow condition, local Nusselt number for heat transfer fluid is obtained from the equation defined by Gnielinski (1976).

Table 3.2 Infinite series solution functions for the circular tube

n	λ_n^2	G_n
0	7.312	0.749
1	44.62	0.544
2	113.8	0.463
3	215.2	0.414
4	348.5	0.382

3.3.2 Non-dimensional Form of Pipe Wall Equation

Dimensionless form of the Equation (3.19) can be derived by using the variables, in Table 3.1,

$$(\rho c)_w \frac{\partial T^0}{\partial t} = \frac{k_l}{D_i^2}\left[\frac{\partial}{\partial X}\left(K_w \frac{\partial T^0}{\partial X}\right) + \frac{1}{R}\frac{\partial}{\partial R}\left(K_w R \frac{\partial T^0}{\partial R}\right)\right] \tag{3.38}$$

$$\frac{\partial T^0}{\partial \tau} = \frac{D_i^2}{\alpha_f (\rho c)_w}\frac{1}{D_i^2}\frac{k_l}{}\left[\frac{\partial}{\partial X}\left(K_w \frac{\partial T^0}{\partial X}\right) + \frac{1}{R}\frac{\partial}{\partial R}\left(K_w R \frac{\partial T^0}{\partial R}\right)\right] \tag{3.39}$$

$$\frac{\partial T^0}{\partial \tau} = \frac{k_l (\rho c)_l}{\alpha_f (\rho c)_l (\rho c)_w}\frac{1}{}\left[\frac{\partial}{\partial X}\left(K_w \frac{\partial T^0}{\partial X}\right) + \frac{1}{R}\frac{\partial}{\partial R}\left(K_w R \frac{\partial T^0}{\partial R}\right)\right] \tag{3.40}$$

Non-dimensional heat conduction equation for the pipe wall can be signified as,

$$C_w \frac{\partial \theta}{\partial \tau} = \frac{\alpha_l}{\alpha_f}\left[\frac{\partial}{\partial X}\left(K_w \frac{\partial \theta}{\partial X}\right) + \frac{1}{R}\frac{\partial}{\partial R}\left(K_w R \frac{\partial \theta}{\partial R}\right)\right] \tag{3.41}$$

3.3.3 Non-dimensional Form of PCM Equation

Dimensionless form of the Equation (3.20) can be written as follows, from the given variables, in Table 3.1,

$$\frac{\partial \theta}{\partial \tau} = \frac{k_l (\rho c)_l}{\alpha_f (\rho c)_l (\rho c)_s}\frac{1}{}\left[\frac{1}{R}\frac{\partial}{\partial R}\left(KR\frac{\partial \theta}{\partial r}\right) + \frac{\partial}{\partial X}\left(K\frac{\partial \theta}{\partial X}\right)\right] - \frac{dS(\rho c)_l}{d\tau (\rho c)_s} \tag{3.42}$$

$$\frac{\partial (C\theta)}{\partial \tau} = \frac{\alpha_l}{\alpha_f}\left[\frac{1}{R}\frac{\partial}{\partial R}\left(KR\frac{\partial \theta}{\partial r}\right) + \frac{\partial}{\partial X}\left(K\frac{\partial \theta}{\partial X}\right)\right] - \frac{dS}{d\tau} \tag{3.43}$$

where, $K(\theta)$, $C(\theta)$, $S(\theta)$ terms are defined in dimensionless form as follows,

$$C = C(\theta) = \begin{cases} C_{sl} & \theta < -\delta\theta_m \quad \text{Solid} \\ \left(\frac{1}{2}(1+C_{sl}) + \frac{1}{2Ste\delta\theta_m}\right) & -\delta\theta_m \le \theta \le \delta\theta_m \quad \text{Mushy} \\ 1 & \theta > \delta\theta_m \quad \text{Liquid} \end{cases} \tag{3.44}$$

$$S = S(\theta) = \begin{cases} C_{sl}\delta\theta_m & \theta < -\delta\theta_m \quad \text{Solid} \\ \left(\frac{1}{2}\delta\theta_m(1+C_{sl}) + \frac{1}{2Ste}\right) & -\delta\theta_m \le \theta \le \delta\theta_m \quad \text{Mushy} \\ C_{sl}\delta\theta_m + \frac{1}{Ste} & \theta > \delta\theta_m \quad \text{Liquid} \end{cases} \tag{3.45}$$

$$K = K(\theta) = \begin{cases} K_{sl} & \theta < -\delta\theta_m \quad \text{Solid} \\ K_{sl} + \frac{(1-K_{sl})(\theta+\delta\theta_m)}{2\delta\theta_m} & -\delta\theta_m \le \theta \le \delta\theta_m \quad \text{Mushy} \\ 1 & \theta > \delta\theta_m \quad \text{Liquid} \end{cases} \tag{3.46}$$

3.4 The Related Initial and Boundary Conditions

The initial and boundary conditions are defined for the solution domain, as follows,

Initial conditions: $(\tau = 0)$

$$0 \le X \le L/D, \quad 0 \le R \le R_{\inf} \quad \rightarrow \quad \theta = \theta_i \tag{3.47a}$$

Boundary Conditions: $(\tau > 0)$

$$X = 0, \quad 0 < R < 0.5 \quad \rightarrow \quad \theta = \theta_{in} = -1 \tag{3.47b}$$

$$X = 0, \quad 0.5 < R < R_{\inf} \quad \rightarrow \quad \frac{\partial\theta}{\partial X} = 0 \tag{3.47c}$$

$$0 \le X \le L/D, \quad R = R_{\inf} \quad \rightarrow \quad \left.\frac{\partial\theta}{\partial R}\right|_{R=R_{\inf}} = 0 \tag{3.47d}$$

$$X = L/D, \quad 0 < R < R_{\inf} \quad \rightarrow \quad \frac{\partial\theta}{\partial X} = 0 \tag{3.47e}$$

As a summary of the numerical model, dimensionless form of governing equations for each subsection and boundary conditions of the system are represented on the mathematical model together, in Figure 3.6.

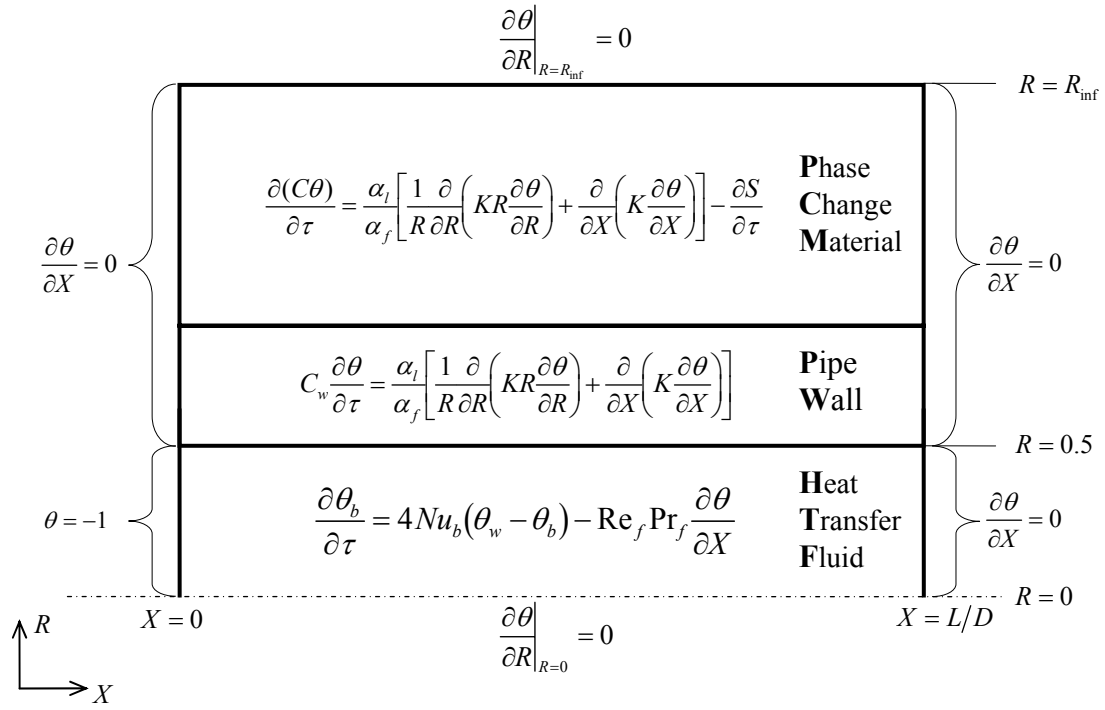

Figure 3.6 Governing equations and boundary conditions for mathematical model

3.5 Control-Volume Formulation and Discretization

Discretization equations of a computational domain can be derived from the governing equations in many ways,

- Finite difference,
- Finite element,
- Spectral methods,
- Finite volume (*control volume*) method,

As an outline, the basis of the solver methods perform the following steps (Versteeg and Malalasekera, 1995),

- Approximation of the unknown flow variables by means of simple functions,
- Discretization by substitution of the approximations into the governing flow equations and subsequent mathematical manipulations,
- Solution of the algebraic equations.

3.5.1 Control-Volume Formulation

Control volume formulation is useful tool for discretizing the differential equations, and the most attractive feature of the control-volume formulation is that the resulting solution would imply that the integral conversation of the quantities such as mass, momentum, and energy is exactly satisfied over any group of control volumes and, naturally, over the whole calculation domain. (Patankar 1980)

In this method the calculation domain is divided into a number of non-overlapping control volumes (Figure 3.7) such that there is one control volume surrounding each grid point. The differential equation is integrated over each control volume. Piecewise profiles expressing the variation of ϕ between the grid points are used to evaluate the required integrals. The result is the discretization equation containing the values of ϕ for a group of grid points. The discretization equation obtained in this manner expresses the conservation principle for ϕ for the finite control volume, just as the differential equation expresses it for an infinitesimal control volume. (Patankar 1980)

$$\begin{bmatrix}\text{Rate of change of}\\ \phi \text{ in the control volume}\\ \text{with respect time}\end{bmatrix} = \begin{bmatrix}\text{Net flux of } \phi \text{ due}\\ \text{to convection into}\\ \text{the control volume}\end{bmatrix} + \begin{bmatrix}\text{Net flux of } \phi \text{ due}\\ \text{to diffusion into}\\ \text{the control volume}\end{bmatrix} + \begin{bmatrix}\text{Net rate of creation of}\\ \phi \text{ inside the control}\\ \text{volume}\end{bmatrix}$$

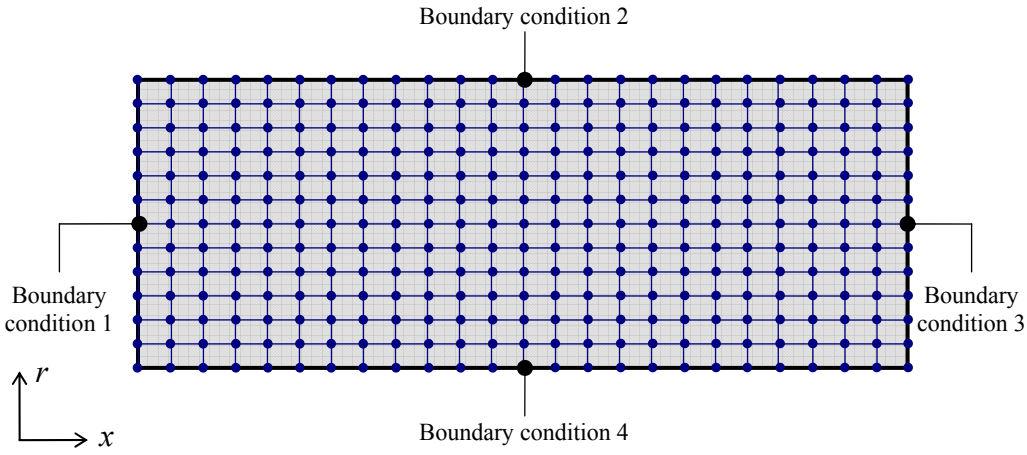

Figure 3.7 Grid layout for a computation domain with its boundary conditions

3.5.2 Discretization for Two Dimensional Control Volume

Control volume approach and discretization of governing equation can be explained via an illustrative example. Because of its simplicity, discretizing a steady and two-dimensional diffusion equation for cylindrical coordinate is selected. Governing equation of the problem is, well-known diffusion equation,

$$\frac{\partial}{\partial x}\left(\Gamma\frac{\partial\phi}{\partial x}\right)+\frac{1}{r}\frac{\partial}{\partial r}\left(\Gamma r\frac{\partial\phi}{\partial r}\right)+S=0 \qquad (3.48)$$

where, ϕ is diffusion property, *e.g. temperature*, Γ is the diffusion coefficient, *e.g. thermal conductivity* and S is the source term, *e.g. the rate of heat generation per unit volume*.

The first step in the finite volume method is to divide the domain into discrete control volumes. Discretization equation can be derived for the grid-point cluster, shown in Figure 3.8. Here the central point of the control volume is indicated with P, and the nodes to the west and east, are identified by W and E respectively. The northern and southern neighbors of the central point are represented by N and S. Bold border lines show the faces of the control volume, and e, w, n, s denote these

faces. For the two-dimensional problem under consideration, we shall assume a unit angle (Versteeg and Malalasekera, 1995).

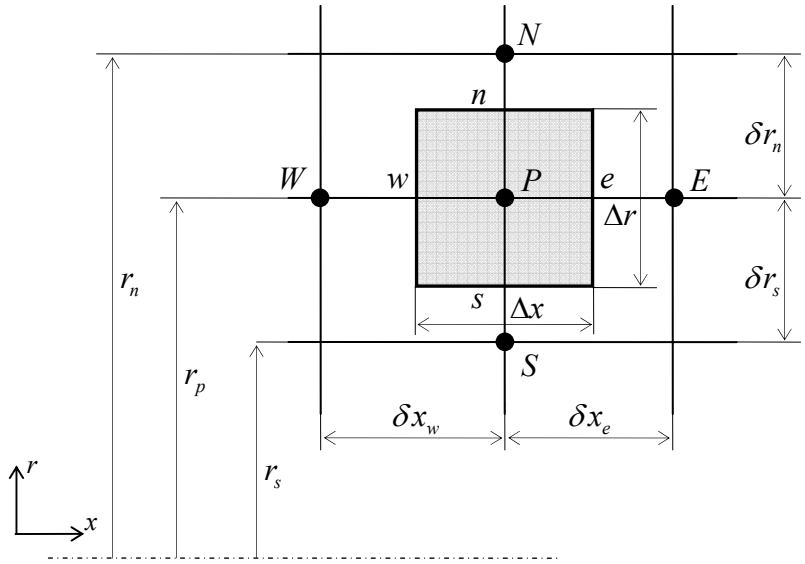

Figure 3.8 Control volume and grid nodes for two-dimensional domain

The key step of the finite volume is the integration of the governing equation (or equations) over a control volume to yield a discretized equation at its nodal point P (Versteeg and Malalasekera, 1995). Integration of the Equation (3.48) over the control volume, as above-mentioned, can be written as follows,

$$\iiint_V \frac{\partial}{\partial x}\left(\Gamma \frac{\partial \phi}{\partial x}\right) dV + \iiint_V \frac{1}{r}\frac{\partial}{\partial r}\left(\Gamma r \frac{\partial \phi}{\partial r}\right) dV + \iiint_V S dV = 0 \tag{3.49}$$

where the differential volume is,

$$dV = 2\pi dr dx \tag{3.50}$$

so,

$$\iiint_V \frac{\partial}{\partial x}\left(\Gamma \frac{\partial \phi}{\partial x}\right) r dr dx + \iiint_V \frac{1}{r}\frac{\partial}{\partial r}\left(\Gamma r \frac{\partial \phi}{\partial r}\right) r dr dx + \iiint_V S r dr dx = 0 \tag{3.51}$$

Here, linear interpolation functions are used between the grid points, hence, derivatives $d\phi/dx$ and $d\phi/dr$ can be written from the piecewise-linear profile,

$$\left[\left(\Gamma\frac{\partial\phi}{\partial x}\right)_e-\left(\Gamma\frac{\partial\phi}{\partial x}\right)_w\right]r_p'\Delta r+\left[\left(\Gamma r\frac{\partial\phi}{\partial r}\right)_n-\left(\Gamma r\frac{\partial\phi}{\partial r}\right)_s\right]\Delta x+\bar{S}\Delta V=0 \tag{3.52}$$

In Equation (3.52), $\bar{S}$ is the average value of the source over the control volume, and the diffuse flux terms are evaluated as,

$$\left(\Gamma\frac{\partial\phi}{\partial x}\right)_e=\Gamma_e\left(\frac{\phi_E-\phi_P}{\delta x_e}\right) \tag{3.53a}$$

$$\left(\Gamma\frac{\partial\phi}{\partial x}\right)_w=\Gamma_w\left(\frac{\phi_P-\phi_W}{\delta x_w}\right) \tag{3.53b}$$

$$\left(\Gamma r\frac{\partial\phi}{\partial r}\right)_n=\Gamma_n\left(r_n\frac{\phi_N-\phi_P}{\delta r_n}\right) \tag{3.53c}$$

$$\left(\Gamma r\frac{\partial\phi}{\partial r}\right)_s=\Gamma_s\left(r_s\frac{\phi_P-\phi_S}{\delta r_s}\right) \tag{3.53d}$$

The source term S may be a function of the dependent variable, in such cases, the finite volume method approximates the source term by means of a linear form;

$$\bar{S}\Delta V=S_u+S_P\phi_P \tag{3.54}$$

Equations (3.53a) to (3.54) can be arranged in Equation (3.52),

$$\left[\Gamma_e\left(\frac{\phi_E-\phi_P}{\delta x_e}\right)-\Gamma_w\left(\frac{\phi_P-\phi_W}{\delta x_w}\right)\right]r_p'\Delta r+\left[\Gamma_n\left(r_n\frac{\phi_N-\phi_P}{\delta r_n}\right)-\Gamma_s\left(r_s\frac{\phi_P-\phi_S}{\delta r_s}\right)\right]\Delta x+\left(S_u+S_P\phi_P\right)=0 \tag{3.55}$$

here, r_p' is defined as, $r_p' = \frac{r_n + r_s}{2}$, and Γ is used to represent the value of Γ pertaining to the particular control face, e.g. Γ_e refers to interface e If the diffusion coefficient Γ is a function of x, then the value of Γ must be known at the grid points N, S, E and P and so on (Erek, 1999).

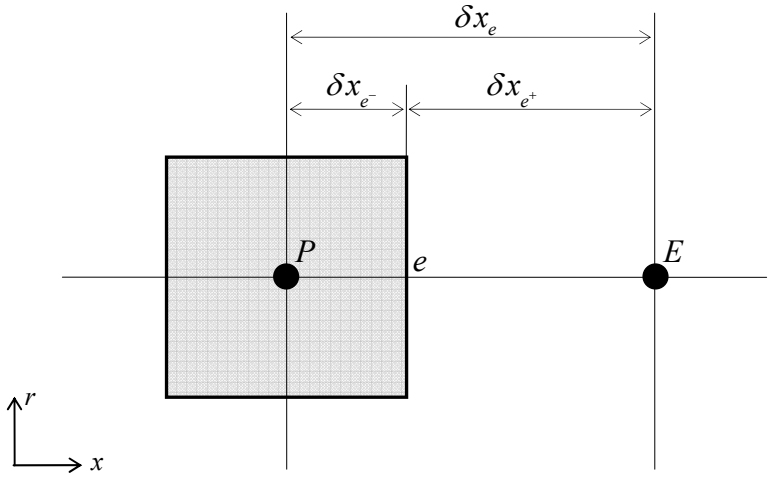

Figure 3.9 Distances for interface e

The interpolation factor f_e is a ratio defined in terms of the distances in Figure 3.9;

$$f_e = \frac{\delta x_{e^+}}{\delta x_e} \tag{3.56}$$

if the interface e is the midway between the grid points, f_e would be 0.5, and Γ_e would be arithmetic mean of Γ_P and Γ_E.

Heat flux equations for interface e can be obtained as,

$$q_e = \Gamma_e \frac{T_P - T_E}{\delta x_e} \tag{3.57}$$

and another flux equation can be written, if the control volume that surround the grid point P is filled with a material of uniform diffusion coefficient Γ_P, and the one around E with a material of diffusion coefficient Γ_E, so the steady heat flux for the composite slab between the points P and E leads to,

$$q_e = \frac{T_P - T_E}{\delta x_e / \Gamma_P + \delta x_{e^+} / \Gamma_E} \tag{3.58}$$

Equations (3.57) and (3.58) can be arranged to express the desired Γ_e,

$$\Gamma_e = \left(\frac{1 - f_e}{\Gamma_P} + \frac{f_e}{\Gamma_E} \right)^{-1} \tag{3.59}$$

As a particular grid structure, if the interface e is placed midway between P and E, then interpolation factor becomes, $f_e = 0.5$. So the Equation (3.59) can be re-arranged as follows,

$$\Gamma_e^{-1} = 0.5 \left(\frac{1}{\Gamma_P} + \frac{1}{\Gamma_E} \right) \quad \text{or} \quad \Gamma_e = \frac{2\Gamma_P \Gamma_E}{\Gamma_P + \Gamma_E} \tag{3.60}$$

Thus, Γ_e is gained as a harmonic mean of Γ_P and Γ_E, rather than the arithmetic mean, for uniform grid. (Patankar 1980).

Equation (3.55) can be re-arranged to obtain the general form,,

$$\left(\frac{\Gamma_e}{\delta x_e} r_p' \Delta r + \frac{\Gamma_w}{\delta x_w} r_p' \Delta r + \frac{\Gamma_n}{\delta r_n} r_n \Delta x + \frac{\Gamma_s}{\delta r_s} r_s \Delta x - S_P \right) \phi_P = \left(\frac{\Gamma_w}{\delta x_w} r_p' \Delta r \right) \phi_W + \left(\frac{\Gamma_e}{\delta x_e} r_p' \Delta r \right) \phi_E + \left(\frac{\Gamma_n}{\delta r_n} r_n \Delta x \right) \phi_N + \left(\frac{\Gamma_s}{\delta r_s} r_s \Delta x \right) \phi_S + S_u \tag{3.61}$$

The coefficients of ϕ_W, ϕ_E, ϕ_N and ϕ_S in Equation (3.61) can be defined as a_W, a_E, a_N and a_S and the coefficient of ϕ_P as a_P, hence the general form of the discretized equation can be written as

$$a_P\phi_P = a_W\phi_W + a_E\phi_E + a_N\phi_N + a_S\phi_S + S_u \tag{3.62}$$

with,

a_W	a_E	a_N	a_S	a_P	b
$\frac{\Gamma_e}{\delta x_e} r_p' \Delta r$	$\frac{\Gamma_w}{\delta x_w} r_p' \Delta r$	$\frac{\Gamma_n}{\delta r_n} r_n \Delta x$	$\frac{\Gamma_s}{\delta r_s} r_s \Delta x$	$a_W + a_E + a_N + a_S - S_P$	S_u

The values of S_u and S_P can be get from source model as given in Equation (3.54). Equations (3.55) and (3.62) represent the discretized form of the Equation (3.48). (Patankar 1980)

Thus, set of algebraic equations can be obtained by means of discretizing the governing equations related to the boundary conditions to obtain the ϕ distribution of the solution domain, as in Figure 3.7. The boundary side coefficient is set to zero and the flux crossing the boundary is introduced such a source term which is appended to any existing S_u and S_P terms. This process results a system of linear algebraic equations which needs to be solved. The complexity and size of the set of equations depends on the dimensionality of the problem, the number of grid nodes and the discretization practice (Versteeg and Malalasekera, 1995).

To solve the algebraic equations, there exist several computer algorithms which are divided into two main groups of solution techniques;

- *Direct methods* (requiring no iteration)
- *Indirect methods* (or iterative methods).

For linear problems, which require the solution of algebraic equations only once, that arise N equations with N unknowns, direct methods may be appropriate. Besides, for two- or three- dimensional problems, solving the algebraic equations becomes more complicated and requires rather large amounts of computer memory and time. Common used examples of direct methods are *Cramer's rule matrix inversion* and *Gaussian elimination*. (Patankar 1980; Versteeg and Malalasekera, 1995)

On the other hand, iterative methods are based on the repeated application of a relatively simple algorithm leading to eventual convergence after a –sometimes large– number of repetitions. Well–known examples are the *Jacobi* and *Gauss–Seidel* iterative methods. In simple computer programs, this method can be useful; however, they can be slow to converge when the system of equations is large. Thomas (1949) developed a technique for rapidly solving tri-diagonal systems that is called Thomas algorithm or *Tri-Diagonal Matrix Algorithm* (TDMA). In addition to this, there are several methods that have been developed recently, such as, *Strongly Implicit procedure* (SIP) by Stone (1968), *Conjugate Gradient Method* (CGM) by Hestenes and Steifel (1952), and *Strongly Implicit Solver* (SIS) by Lee (1989).

In this study SIS algorithm is used, due to it is computationally inexpensive and having the advantage that it required a minimum amount of storage (Versteeg and Malalasekera, 1995). Detailed information is given in *Appendixes A.1* for S.I.S. algorithm.

3.6 Discretization of Governing Equations

Dimensionless governing equations were obtained as summarized in Figure 3.6. These differential equations are turned into discretization equations via control volume approach as discussed above.

3.6.1 Discretization of HTF Equation

Dimensionless heat transfer equation for heat transfer fluid (HTF) was defined as Equation (3.35). For any control volume (Figure 3.10) from the inner nodes of the solution domain for the HTF, discretized equation can be obtained for nodal point P, with integration of the governing equation over a control volume,

$$\iint_{V,\tau}\frac{\partial\theta}{\partial\tau}d\tau dV=\iint_{\tau,V}4Nu\left(\theta_w-\theta_f\right)dVd\tau-\iint_{\tau,V}\mathrm{PrRe}\frac{\partial\theta}{\partial X}dVd\tau \tag{3.63}$$

$$\frac{\theta_P-\theta_P^0}{\Delta\tau}=4Nu\left(\theta_N-\theta_P\right)-Pe\frac{\left(\theta_e-\theta_w\right)}{\Delta X} \tag{3.64}$$

Here, the temperature values at a cell face are assumed that equal to the value at the upstream node via Equation (3.65). When the flow is in the positive direction, as illustrated in Figure 3.10, $u_w>0$, $u_e>0$ ($F_w>0$, $F_e>0$), the upwind scheme sets (Versteeg and Malalasekera, 1995),

$$T_w=T_W \text{ and } T_e=T_p \tag{3.65}$$

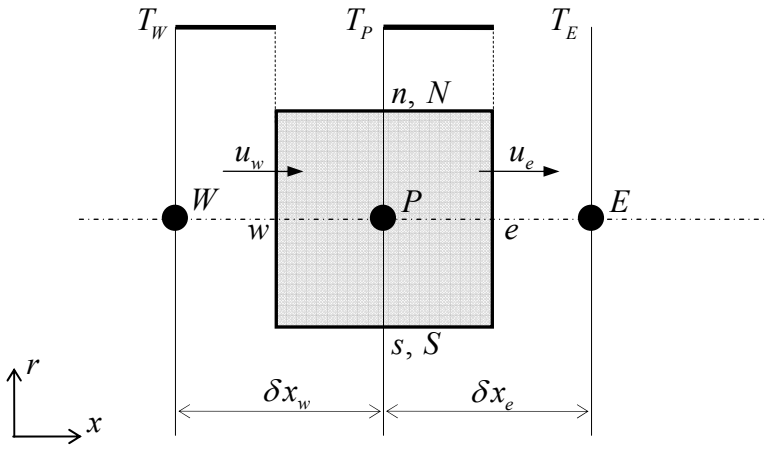

Figure 3.10 Nodal values for HTF

and the discretized equation becomes,

$$\frac{\theta_P - \theta_P^0}{\Delta\tau} = 4Nu\left(\theta_N - \theta_P\right) - Pe\frac{\left(\theta_P - \theta_W\right)}{\Delta X} \tag{3.66}$$

it can be re-arranged to convert into general form,

$$\left(\frac{1}{\Delta\tau} + 4Nu\right)\theta_P = \left(4Nu\right)\theta_N + \left(\frac{Pe}{\Delta X}\right)\theta_W + \left(\frac{1}{\Delta\tau}\right)\theta_P^0 \tag{3.67}$$

General form of the discretized equation for nodal points can be written as,

$$a_P\theta_P = a_W\theta_W + a_E\theta_E + a_N\theta_N + a_S\theta_S + a_P^0\theta_P^0 \tag{3.68}$$

with the coefficients of,

$$a_W = Pe/\Delta X\ ,\ a_E = 0\ ,\ a_N = 4Nu\ ,\ a_S = 0\ ,\ a_P^0 = 1/\Delta\tau$$
$$a_P = a_W + a_E + a_N + a_S + a_P^0 \tag{3.69}$$

3.6.2 Discretization of Pipe Wall Equation

Dimensionless heat transfer equation for the pipe wall section was defined as in Equation (3.41). For any control volume (Figure 3.8) from the inner nodes of the solution domain for the pipe wall, discretized equation can be obtained for nodal point P, with integration of the governing equation over a control volume,

$$C_w \iint_{V,\tau} \frac{\partial\theta}{\partial\tau} d\tau dV = \frac{\alpha_l}{\alpha_f}\left[\iint_{\tau,V} \frac{\partial}{\partial X}\left(K_w \frac{\partial\theta}{\partial X}\right) dV d\tau + \iint_{\tau,V} \frac{1}{R}\frac{\partial}{\partial R}\left(K_w R \frac{\partial\theta}{\partial R}\right) dV d\tau\right] \tag{3.70}$$

$$C_w \frac{\theta_P - \theta_P^0}{\Delta\tau} R_P' \Delta R \Delta X = C_2\left[\left(K_n R_n \frac{\theta_N - \theta_P}{\delta R_n} - K_s R_s \frac{\theta_P - \theta_S}{\delta R_s}\right)\Delta X + \left(K_e \frac{\theta_E - \theta_P}{\delta X_e} - K_w \frac{\theta_P - \theta_W}{\delta X_w}\right) R_P' \Delta R\right] \tag{3.71}$$

where, $C_2 = \alpha_l/\alpha_f$

General form of the discretized equation for nodal points can be written as,

$$a_P\theta_P = a_W\theta_W + a_E\theta_E + a_N\theta_N + a_S\theta_S + a_P^0\theta_P^0$$

for the coefficients of,

$$a_W = C_2K_wR'_P\Delta R/\delta X_w\ ,\ a_E = C_2K_eR'_P\Delta R/\delta X_e$$
$$a_N = C_2K_nR_n\Delta X/\delta R_n\ ,\ a_S = C_2K_sR_s\Delta X/\delta R_s\ ,\ a_P^0 = C_wR'_P\Delta X\Delta R/\Delta\tau$$
$$a_P = a_W + a_E + a_N + a_S + a_P^0 \qquad (3.72)$$

3.6.3 Discretization of Pipe Wall – HTF Interface Equation

For pipe wall–HTF interface section, heat transfer equation differs from Equation (3.41), because of the convection effects. For a control volume for interface section, Figure (3.11), the energy equation can be written from the Equation (3.19),

$$(\rho c)_w\frac{\partial T^0}{\partial t} = \frac{\partial}{\partial x}\left(k_w\frac{\partial T^0}{\partial x}\right) + \frac{1}{r}\frac{\partial}{\partial r}\left(k_w r\frac{\partial T^0}{\partial r}\right)$$

with the boundary condition for node P,

$$k_w\left.\frac{\partial T}{\partial r}\right|_P = h\left(T_P - T_S\right) \qquad (3.73)$$

and dimensional energy equation can be arranged to obtain the non-dimensional form,

$$C_w\frac{\theta_P - \theta_P^0}{\Delta\tau}R'_P\Delta R\Delta X = C_2\left[\left(K_nR_n\frac{\theta_N - \theta_P}{\delta R_n} - 0.5NuK_f\left(\theta_P - \theta_S\right)\right)\Delta X + \left(K_e\frac{\theta_E - \theta_P}{\delta X_e} - K_w\frac{\theta_P - \theta_W}{\delta X_w}\right)R'_P\Delta R\right] \qquad (3.74)$$

General form of the discretized equation for nodal points can be written as,

$$a_P\theta_P = a_W\theta_W + a_E\theta_E + a_N\theta_N + a_S\theta_S + a_P^0\theta_P^0$$

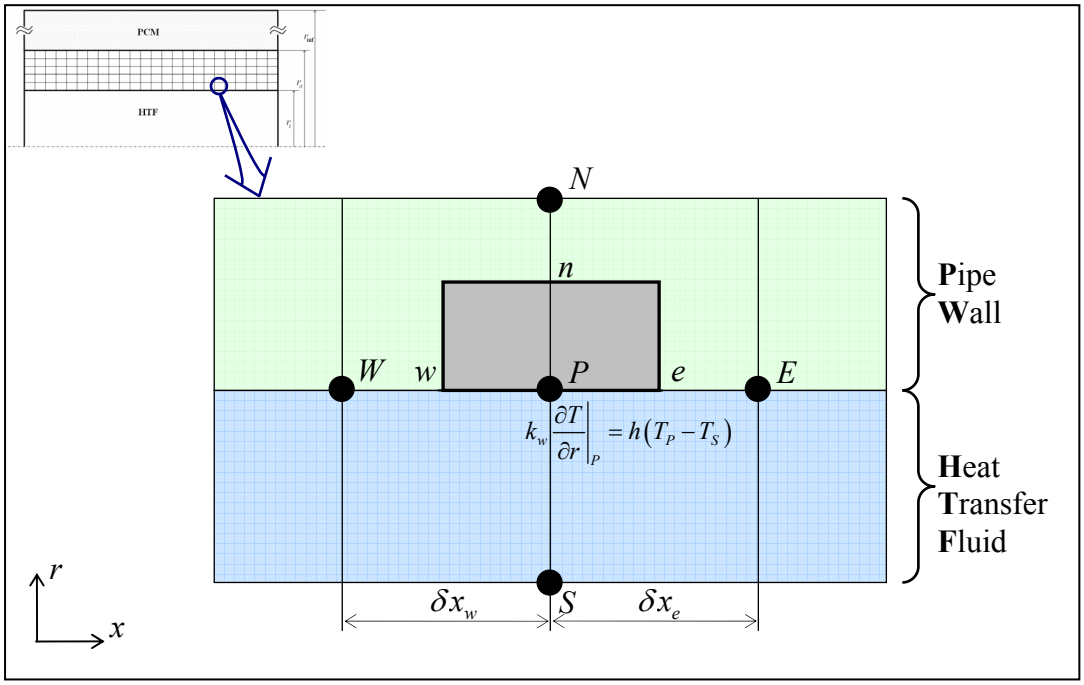

Figure 3.11 Control volume for interface between HTF and pipe wall

for the coefficients of,

$$a_W = C_2 K_w R'_P \Delta R / \delta X_w \,,\; a_E = C_2 K_e R'_P \Delta R / \delta X_e$$

$$a_N = C_2 K_n R_n \Delta X / \delta R_n \,,\; a_S = 0.5 Nu C_2 \Delta X \,,\; a_P^0 = C_w R'_P \Delta X \Delta R / \Delta\tau$$

$$a_P = a_W + a_E + a_N + a_S + a_P^0 \qquad (3.75)$$

3.6.4 Discretization of PCM Equation

Dimensionless heat transfer equation for PCM is defined as Equation (3.43). For any control volume (Figure 3.8) from the inner nodes of the solution domain for the PCM section, discretized equation can be obtained for nodal point P, with integration of the governing equation over a control volume,

$$C\iint_{V,\tau}\frac{\partial\theta}{\partial\tau}d\tau dV=\frac{\alpha_l}{\alpha_f}\left[\iint_{\tau,V}\frac{1}{R}\frac{\partial}{\partial R}\left(KR\frac{\partial\theta}{\partial r}\right)dVd\tau+\iint_{\tau,V}\frac{\partial}{\partial X}\left(K\frac{\partial\theta}{\partial X}\right)dVd\tau\right]-\iint_{V,\tau}\frac{dS}{d\tau}d\tau dV \quad (3.76)$$

$$C\frac{\theta_P-\theta_P^0}{\Delta\tau}R'_P\Delta R\Delta X=\left[K_e\frac{\theta_E-\theta_P}{\delta X_e}-K_w\frac{\theta_P-\theta_W}{\delta X_w}\right]C_2R'_P\Delta R+\left[K_nR_n\frac{\theta_N-\theta_P}{\delta R_n}-K_sR_s\frac{\theta_P-\theta_S}{\delta R_s}\right]$$
$$C_2\Delta X-\frac{S_P-S_P^0}{\tau}R'_P\Delta R\Delta X \quad (3.77)$$

General form of the discretized equation for nodal points can be written as,

$$a_P\theta_P=a_W\theta_W+a_E\theta_E+a_N\theta_N+a_S\theta_S+a_P^0\theta_P^0$$

for the coefficients of,

$$a_W=C_2K_wR'_P\Delta R/\delta X_w,\ a_E=C_2K_eR'_P\Delta R/\delta X_e$$
$$a_N=C_2K_nR_n\Delta X/\delta R_n,\ a_N=C_2K_sR_s\Delta X/\delta R_s,\ a_P^0=CR'_P\Delta X\Delta R/\Delta\tau$$
$$a_P=a_W+a_E+a_N+a_S+a_P^0 \quad (3.78)$$

where C, K, S coefficients are defined as in Equations (3.44) – (3.46).

As a summary of the discretization of the solution domain for interior nodes, the neighbour coefficients are represented in Table 3.3.

Table 3.3 Central nodes coefficients for solution domain

Domain	**Neighbour coefficients**				
	a_N	a_S	a_E	a_W	a_P^0
Pipe **W**all **(PW)**	$C_2\frac{K_nR_n\Delta X}{\delta R_n}$	$C_2\frac{K_sR_s\Delta X}{\delta R_s}$	$C_2\frac{K_eR'_P\Delta R}{\delta X_e}$	$C_2\frac{K_wR'_P\Delta R}{\delta X_w}$	$C_w\frac{R'_P\Delta X\Delta R}{\Delta\tau}$
HTF	$4Nu$	0	0	$\frac{Pe}{\Delta X}$	$\frac{1}{\Delta\tau}$
PW - HTF Interface	$C_2\frac{K_nR_n\Delta X}{\delta R_n}$	$C_2Nu\Delta X$	$C_2\frac{K_eR'_P\Delta R}{\delta X_e}$	$C_2\frac{K_wR'_P\Delta R}{\delta X_w}$	$C_w\frac{R'_P\Delta X\Delta R}{\Delta\tau}$
PCM	$C_2\frac{K_nR_n\Delta X}{\delta R_n}$	$C_2\frac{K_sR_s\Delta X}{\delta R_s}$	$C_2\frac{K_eR'_P\Delta R}{\delta X_e}$	$C_2\frac{K_wR'_P\Delta R}{\delta X_w}$	$C_w\frac{R'_P\Delta X\Delta R}{\Delta\tau}$

3.7 Mathematical Model

The temperature distribution inside the solution domain can be calculated by solving the discretized non-dimensional coefficients (Table 3.3) for three sub-domains. The grid distribution of the mathematical model is represented in Figure 3.12. Here N represents the number of grids on $r-axis$ and M symbolizes number of grids through $x-axis$. For HTF section, there exists only one control volume, where the radial heat change is neglected. The pipe wall section is formed with uniform grids between $r_i < r < r_o$. Meanwhile, the grid distribution for PCM is selected to be non-uniform structure, a fine grid spacing applied to the region near the pipe wall, where high temperature gradients occur. Hence, the grid interval for PCM is set the size of the grid is 5 % greater than the previous grid size,

$$\Delta r^j = 1.05 \Delta r^{j-1} \tag{3.79}$$

Totally 114 nodes settles in radial coordinate and 100 ($N_{\text{inf}} = 100$) of which are in region of PCM ($r_o < r < r_{\text{inf}}$). The interval count for axial direction is selected to be 168 ($M = 168$).

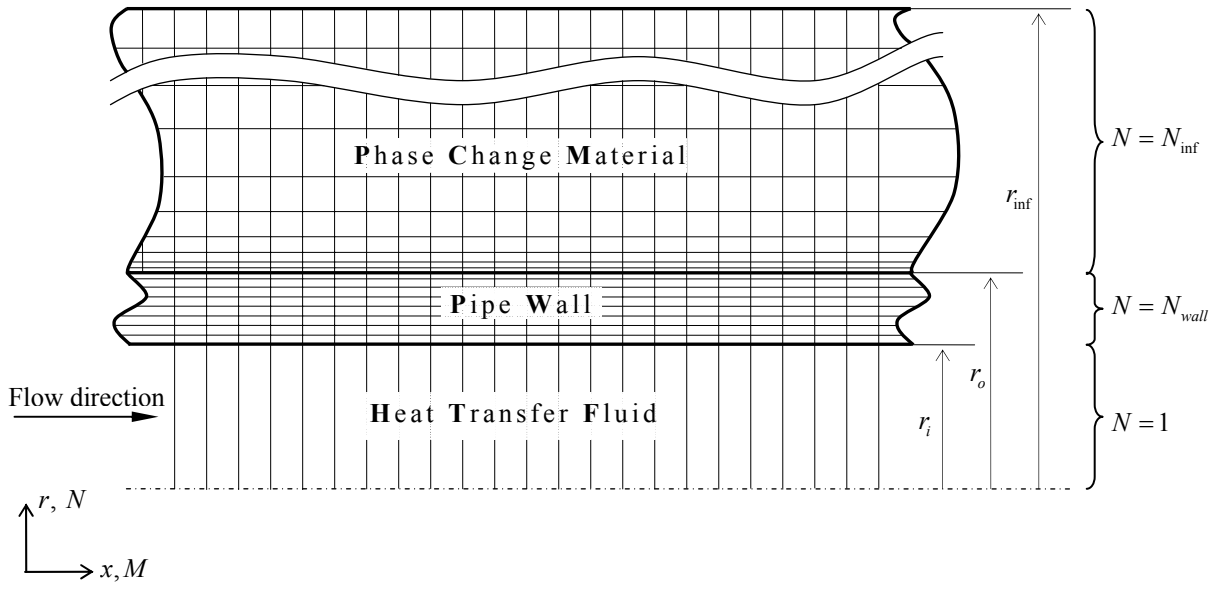

Figure 3.12 The grid used for solution domain

3.8 Computational Algorithm

Strongly implicit solver, (Lee, 1989), is used for solving the discretization forms of energy equations. The advantage of using this solver, is that the CPU time is reduced a great amount for a single iteration and this solver requires less storage than the other solvers. Numerical code is compiled with Intel® Fortran Compiler 9.0, which enables the processor optimization and parallelization for maximizing the use of processor. This modification reduces the computation duration almost 40 %, in comparison with the other compilers.

Numerical code is revised for each analysis depending on the flow conditions such as, flow rate, inlet temperature and also thermo-physical properties. Parameters defined in non-dimensional form as given in Figure 3.6 and Table 3.1.

Since the energy equation occupied by PCM is a non–linear heat conduction equation, iterations are needed during each time step. For a given time step, convergence is declared at the $k+1^{th}$ iteration when $\left|\theta_{i,j}^{k+1}-\theta_{i,j}^{k}\right| \le 10^{-5}$. The accuracy of the solution depends upon the time steps and it is selected to be small interval such as, $\Delta t = 10$ s.

The overall energy balance is checked during the calculation process to verify the numerical results. At a time step, the change in the stored energy of the PCM and pipe must be equal to the total energy supplied by the heat transfer fluid as follows,

$$\int_0^{\tau} \frac{\pi}{4} Pe_f C_f (\theta_{b,out}+1) d\tau = \int_0^{L}\int_{R_i}^{R_{out}} 2\pi R(H-H_i) dR dX \qquad (3.80)$$

The left side of Equation (3.80) represents the thermal energy supplied by the heat transfer fluid while the right side represents the thermal stored energy in the PCM and tube. In calculations, the numerical deviation between two sides of Equation (3.80) is taken to be less than 2 %.

3.9 Numerical Code Validation

Validation of the numerical model checked in two ways. Figure 3.13 shows the time dependent energy storage inside the tank for numerical results in comparison with the experimental results. On the other hand, ice formation around the pipe is also given in comparison with the experimental results, as shown in Figure 3.14, where the ice profile around the pipe through the *x–axis*, is formed as seen in Figure 3.15, so the comparison is given for $x = 3.5\,m$, where the experimental measurements were performed. It can be seen that, there is an agreement between experimental and numerical results, with minor differences, which could arise from the assumptions of the mathematical model such as geometrical simplifications and negligence of the heat lost from the system and the uncertainties of the experiments, such as sensitivity of measuring temperature and little oscillations of volumetric flow rate.

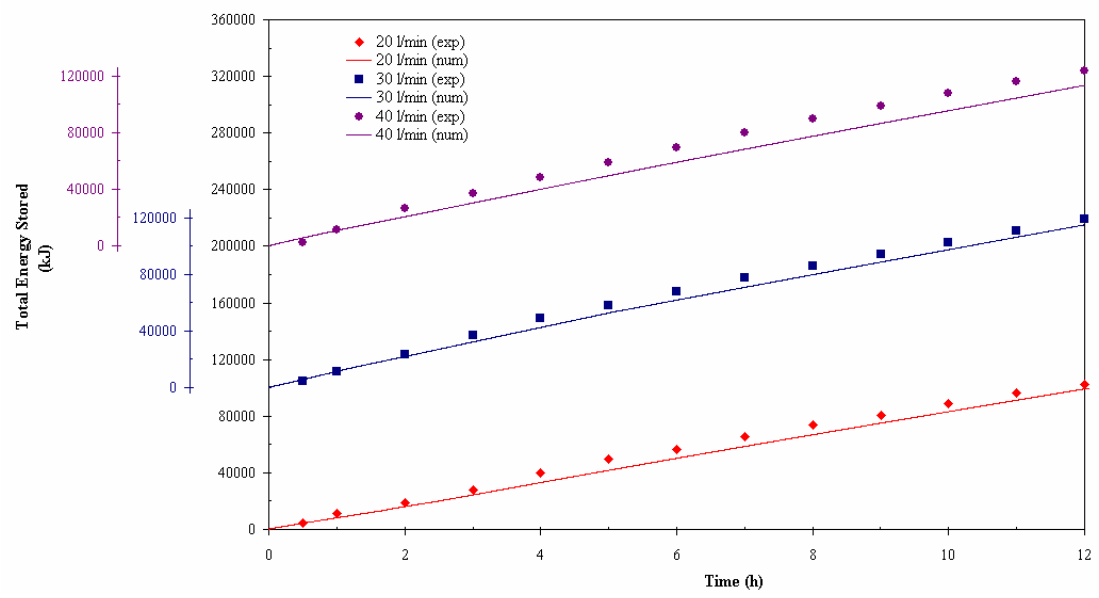

Figure 3.13 Comparisons of numerical and experimental results for three volumetric flow rates

Numerical results become deviated from experimental ones, with the increasing volumetric flow rate, as shown in Figure 3.13. The pipes inside the storage tank have spiral form with lots of elbows, as shown in Figure 3.1. Therefore the flow becomes turbulent at low Reynolds number, while the flow is considered as laminar in

mathematical model. This effect has been shown for high volumetric flow rates and minor differences exist between the numerical and experimental results, especially for high flow rates, such as 40 l/min.

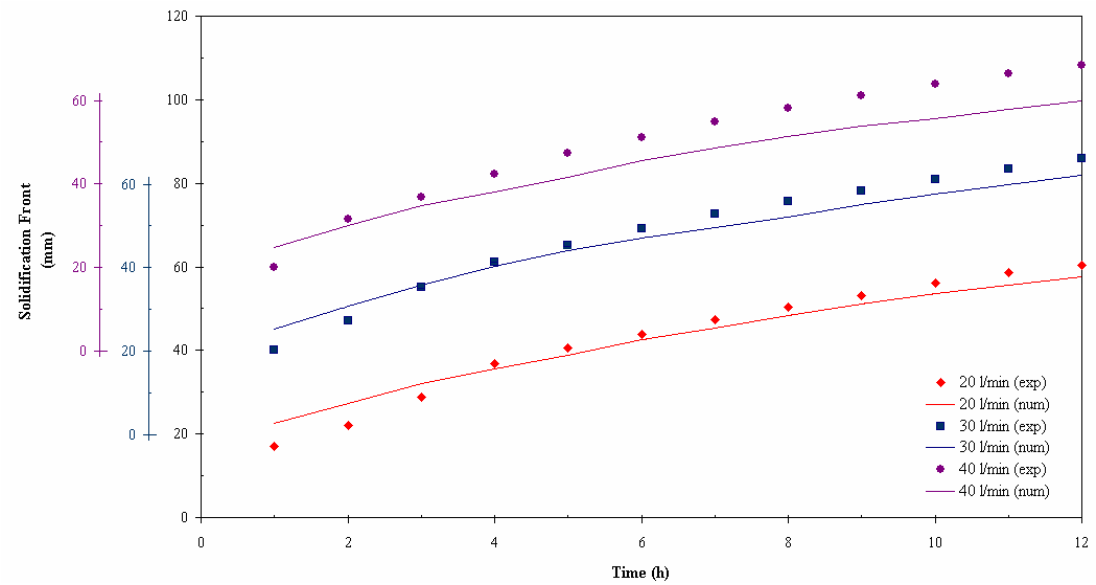

Figure 3.14 Experimental solidification front results in comparison with numerical ones

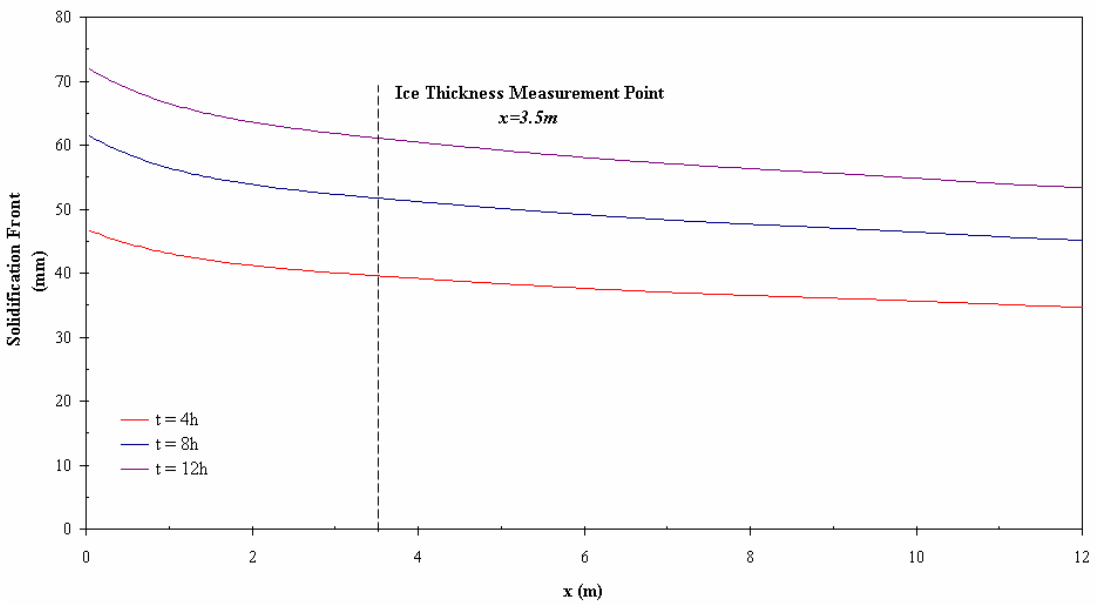

Figure 3.15 Numerical ice profiles through the pipe for 30 l/min

3.10 Numerical Results

After validation of the numerical model, numerical code is used to investigate the effects of volumetric flow rate and inlet temperature on the energy storage.

In order to predict the flow rate effect, the numerical code has been run for five different flow rates, 20 l/min to 60 l/min, which are the minimum and maximum values that the suction pump can supply. In these calculations, the inlet temperature of the secondary coolant and the initial temperature of the system have been set to constant values of –8˚C and 1˚C, respectively. Total stored energy and heat transfer rate results are shown in Figure 3.16 and Figure 3.17. It is obvious that both the energy stored and heat transfer rate raise with increasing flow rate with a decreasing tendency.

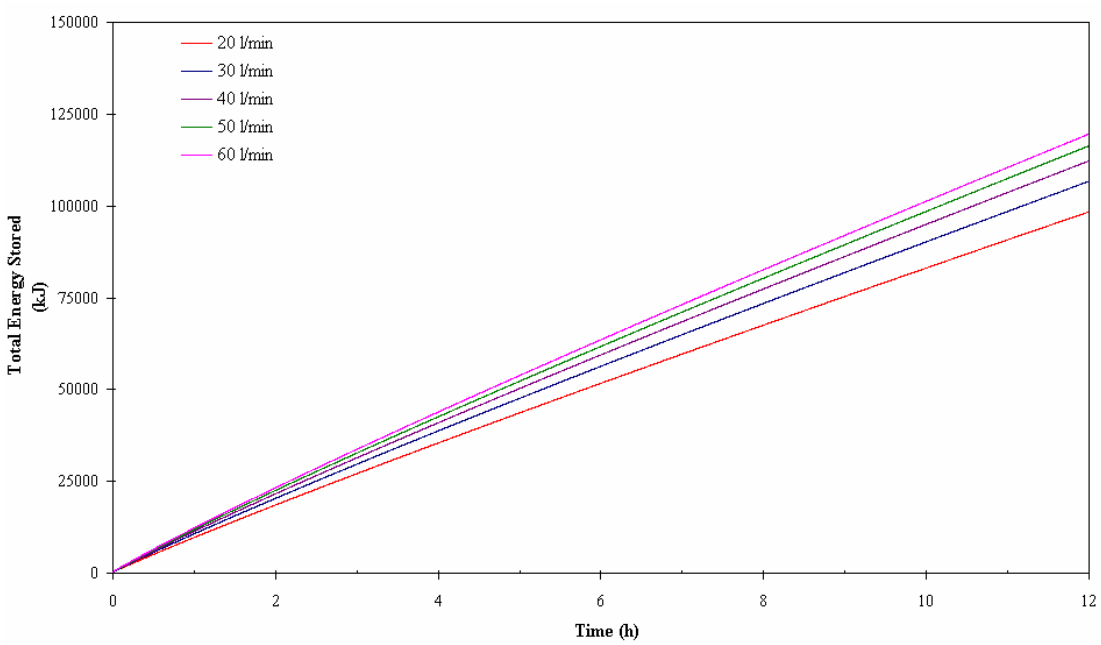

Figure 3.16 The effect of volumetric flow rate on the energy storage

The inlet temperature effect was investigated for a constant volumetric flow rate of 30 l/min at various temperatures namely, –6°C, –8°C and –10°C. It can be seen that, decreasing the inlet temperature raises the stored energy, as shown in Figure 3.18, thus the inlet temperature effect surpasses the flow rate effect.

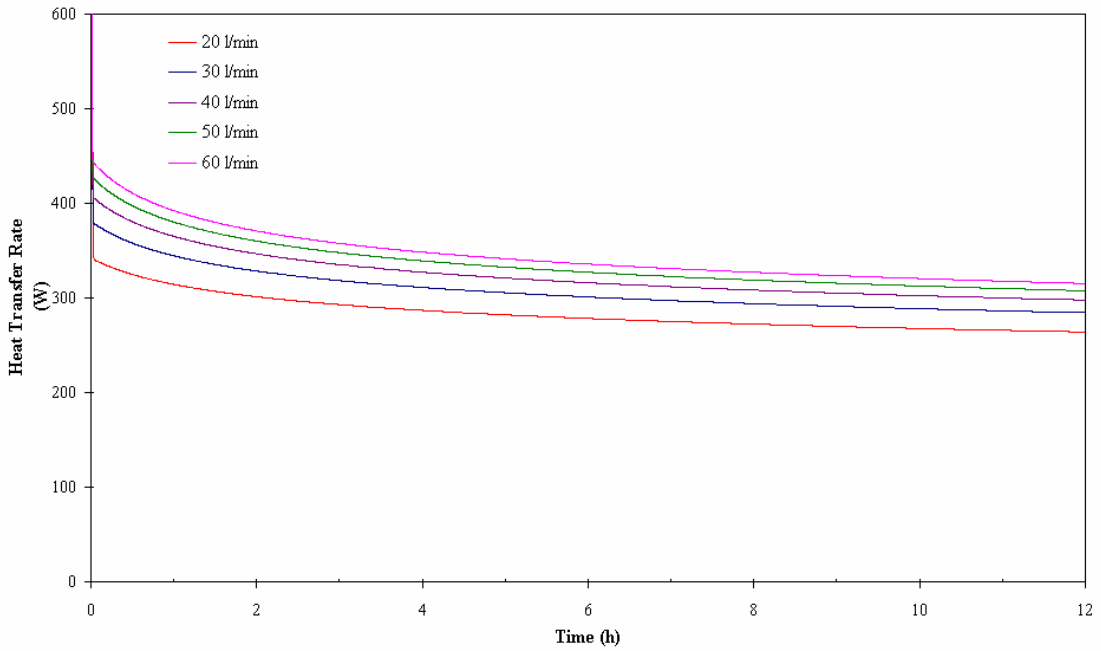

Figure 3.17 Heat transfer rate variation with volumetric flow rate

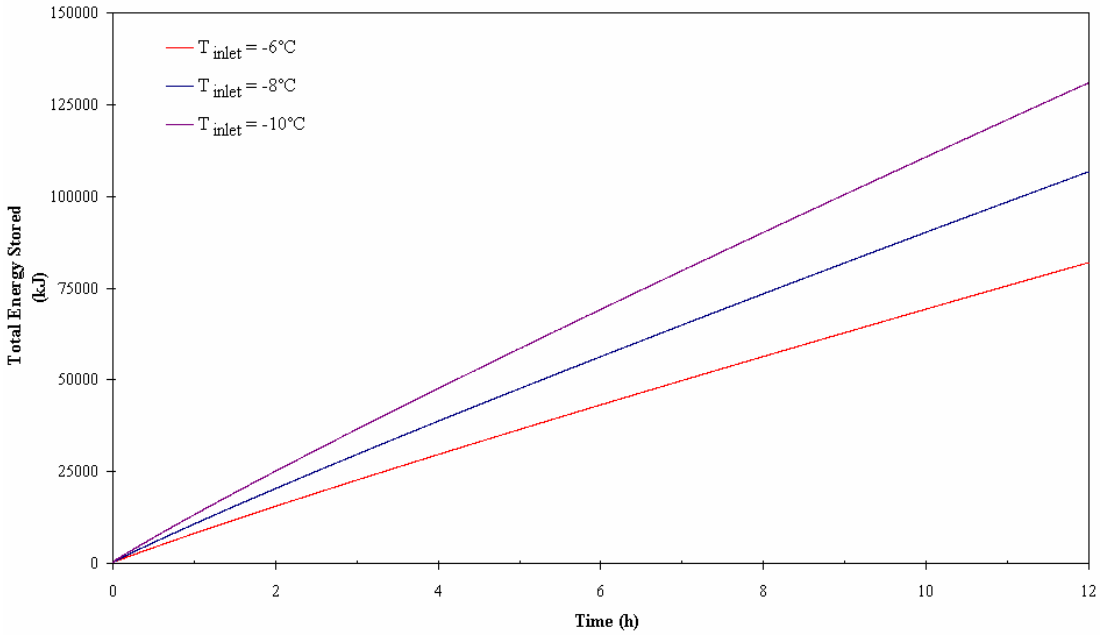

Figure 3.18 The effect of inlet temperature on the stored energy

CHAPTER FOUR
CONCLUSIONS

In this study, a numerical model has been developed for predicting the effects of the flow rate and the inlet temperature of the coolant on the cool storage inside the thermal energy storage system, which consists of ice–on–coil storage tank integrated with chiller. The numerical code has been validated with comprising the experimental results, for both energy stored and solidification front. It is shown that the predictions have a good estimation with the experimental data, especially for relatively low flow rates, so it can be concluded that, the developed numerical method could be efficiently used to simulate the solidification process. There is an agreement between experimental and numerical results, with minor differences, which could arise from the assumptions of the mathematical model such as geometrical simplifications and negligence of the heat lost from the system and the uncertainties of the experiments, as sensitivity of measuring temperature and little oscillations of volumetric flow rate. Numerical results become deviated from experimental ones, with the increasing volumetric flow rate. The pipes inside the storage tank have spiral form with lots of elbows, as shown in Figure 3.1. Therefore the flow becomes turbulent at low Reynolds number, while the flow is considered as laminar in mathematical model. This effect has been shown for high volumetric flow rates and minor differences exist between the numerical and experimental results, especially for high flow rates, such as 40 l/min.

According to present study, following conclusions are obtained;

- For designing an ice–on–coil type thermal energy storage, geometrical parameters are important to obtain the required energy storage, and in addition to this, thermal and flow parameters of the coolant are also key factors for optimization of the system.

- Refrigeration system of the ice storage unit -chiller- has a constant cooling capacity, because of that, flow rate and inlet temperature of the

system has to have an optimum interval to gain maximum energy. According to the Table 2.5, total stored energy rises with increasing the volumetric flow rate from 20 l/min through 40 l/min. Meanwhile, it should not be expected that the stored energy always increases with the increasing flow rate. As seen from the data in Table 2.5; from 40 l/min to 50 l/min, stored energy decreases, since the cooling capacity of the chiller is limited, so the inlet temperature of the coolant rises with the increasing flow rate. This effect can also be seen in Figure 2.6, where the experimental results are given with the bulk inlet temperatures.

- The numerical results show that the stored energy rises with increasing flow rate with a decreasing tendency (Table 4.1), and inlet temperature of the fluid is more influential to increase the energy stored rather than the volumetric flow rate (Table 4.2).

Table 4.1 Volumetric flow rate effect to the energy storage

Hour	**Volumetric flow rate** (l/min)				
(h)	**20**	**30**	**40**	**50**	**60**
1	9731.13	10728.16	11406.58	11915.25	12319.29
2	18576.33	20393.91	21624.55	22544.33	23272.78
3	27123.07	29694.77	31430.33	32724.53	33747.03
4	35465.89	38750.65	40962.44	42608.61	43906.96
5	43655.43	47624.84	50292.48	52274.87	53836.56
6	51723.00	56354.78	59462.52	61770.14	63585.47
7	59689.38	64966.22	68501.89	71124.69	73186.31
8	67570.02	73476.40	77429.89	80360.10	82662.19
9	75375.70	81900.15	86261.79	89493.70	92030.22
10	83115.72	90246.55	95009.70	98536.18	101303.50
11	90796.47	98524.52	103682.24	107498.44	110492.19
12	98423.73	106740.47	112286.78	116388.49	119604.98

Table 4.1 Inlet temperature effect to the energy storage

Hour	**Inlet temperature** (˚C)		
(h)	**-6**	**-8**	**-10**
1	8155.87	10728.16	13260.65
2	15560.17	20393.91	25136.56
3	22703.50	29694.77	36546.02
4	29666.59	38750.65	47648.99
5	36493.18	47624.84	58526.25
6	43210.91	56354.78	69225.98
7	49837.94	64966.22	79780.44
8	56387.88	73476.40	90211.84
9	62870.61	81900.15	100536.35
10	69293.88	90246.55	110767.06
11	75664.42	98524.52	120914.51
12	81986.83	106740.47	130986.63

As a conclusion, in this study, a numerical model has been developed, and verified with experimental investigation. It is shown that, the developed numerical model could be used to design a thermal energy storage unit which includes solidification, to obtain optimum geometrical, flow and thermal conditions.

NOMENCLATURE

A : Area (m^2)

c : specific heat (J kg^{-1} K^{-1})

C^0 : heat capacity (J m^{-3} K^{-1}), $c\rho$

C : dimensionless heat capacity, $C^0/(c_l\rho_l)$

C_{sl} : C_s/C_l

D : diameter (m)

$\dot{E}$: total energy for unit time (W)

f : liquid fraction

h : sensible enthalpy (J m^{-3})convection coefficient (W m^{-2} K^{-1})

H : enthalpy (J kg^{-1})

k : thermal conductivity (W m^{-1} K^{-1})

K : dimensionless thermal conductivity, k/k_l

K_{sl} : k_s/k_l

L : length of pipe (m)

$\dot{m}$: mass flow rate (kg s^{-1})

m : mass (kg)

N : Number of grids on radial axis

Nu : Nusselt number, hD_i/k_f

M : Number of grids on axial axis

Pe : Peclet number, RePr

Pr : Prandtl number, ν_f/α_f

q : heat transfer for unit time (W)

Q : total energy (J)

r : co-ordinate along the radial direction (m)

R : dimensionless co-ordinate along the radial direction, r/D_i

R'' : thermal resistance (m^2 K W^{-1})

Re : Reynolds number, $4\dot{m}/\pi D_i\mu_f$

S^0 : source term

S : dimensionless source term, $S^0/\rho_l c_l\left(T_m^0 - T_{in}^0\right)$

Ste : Stefan number

t : time variable (s)

$\overline{T}$: bulk temperature (K)

T : temperature (K)

T^* : temperature difference, $T - T_m$

$\dot{V}$: volumetric flow rate (l min^{-1})

V : volume (m^3)

x : co-ordinate along the axial direction (m)

X : dimensionless axial direction along axial direction, x/D_i

Greek symbols

α : thermal diffusivity (m^2 s^{-1})

$2\delta T_m$: phase-change temperature range (K)

$2\delta\theta$: dimensionless phase-change temperature range, $\delta T/\left(T_m - T_{in}\right)$

ΔH : energy of fusion (kJ kg^{-1})

ϕ : diffusion property

Γ : diffusion coefficient

θ : dimensionless temperature, $\left(T - T_m\right)/\left(T_m - T_{in}\right)$

ν : kinematic viscosity (m^2 s^{-1})

μ : dynamic viscosity (N s m^{-2})

ρ : density (kg m^{-3})

τ : dimensionless time, $\alpha_f t/D_i^2$

Subscripts

b : bulk

f : transfer fluid

i : initial condition or inside surface of the pipe

in : inlet

inf : outside surface of the thermal storage tank

l : liquid PCM or lateral

lat : latent energy

m : mushy phase or melting point

o : outside surface of the pipe

s : solid PCM

sen : sensible energy

w : container wall (surface) or west interface of the control volume

REFERENCES

Abhat, A. (1983). Low temperature latent heat thermal energy storage: Heat storage materials. *Solar Energy*, 30 313–332.

Asan, H., & Namli, L. (1997). Uncertainty analysis of experimental studies of heat transfer and pressure drops. In: Proceedings of 11th National Heat Science Congress. Edirne: Turkey.

ASHRAE, (1997). *Physical Properties of Secondary Coolants (Brines)*, Fundamentals. Chapter 20.

ASHRAE, (1999). *Thermal Storage*, HVAC Applications. Chapter 33.

Baltimore, (n.d.). *Cooling Towers, Closed Circuit Cooling Towers, Evaporative Condensers, Aircoil Evaporators, Ice Thermal Storage Systems*, Retrieved 20/07/2006, from http://www.baltimoreaircoil.com.

Bellecci, C., & Conti, M. (1993). Phase change thermal storage: transient behaviour analysis of a solar receiver/ storage module using the enthalpy method. *International Journal of Heat Mass Transfer*, 36 2157–2163.

Cabeza, L.F., Roca, J., Noguées. M., Zalba, B., & Marín, J.M. (2002). Transportation and conversation of temperature sensitive materials with phase change materials: state of art, IEA ECES IA Annex 17 2nd Workshop, Ljubljana (Slovenia).

Calmac, (n.d.). *Thermal Energy Storage, Off-Peak Co*., Retrieved 20/07/2006, from http://www.calmac.com.

Cao, Y., & Faghri. A. (1990). A numerical analysis of phase–change problem including natural convection. *ASME Journal of Heat Transfer*, 112 (3), 812–816.

Cao, Y., & Faghri, A. (1991[a]). A PCM/forced convection conjugate transient analysis of energy storage systems with annular and countercurrent flows. *ASME Journal of Heat Transfer*, 113 37–42.

Cao. Y., & Faghri A. (1991[b]). Performance characteristics of a thermal energy storage module: a transient PCM/forced convection conjugate analysis. *International Journal of Heat Mass Transfer*, 34 93–101.

Cao. Y., & Faghri, A. (1992). A study of thermal energy storage system with conjugate turbulent forced convection. *ASME Journal of Heat Transfer*, 114 1019–1027.

Cristopia, (n.d.). *Cristopia Energy Systems,* Retrieved 20/07/2006, from http://www.cristopia.com.

Cryogel, (15/03/2003). *CRYOGEL Thermal Energy Storage,* Retrieved 20/07/2006, from http://www. cryogel.com.

Dincer, I., & Rosen, M.A. (2002). *Thermal Energy Storage: Systems and Applications.* Chichester (England): John Wiley & Sons.

Erek, A. (1999). Phase change around finned horizontal cylinder: a conjugate problem. PhD thesis. İzmir: Graduate School of Natural and Applied Sciences of Dokuz Eylul University.

Erek, A., Başaran, T., Küçüka, S., & Ezan, M.A. (2005[a]). Bir gizli enerji depolama sisteminin deneysel ve teorik olarak incelenmesi. *ULIBTK'05*, Trabzon.

Erek, A., İlken, Z., & Acar, M.A. (2005[b]). Experimental and numerical investigation of thermal energy storage with a finned tube. *International Journal of Energy Resources,* 29 283–301.

Espeau, P., Mondieig, D., Haget, Y., & Cuevas-Diarte, M.A. (1997). 'Active' package for thermal protection of food products. *Packag. Technol. Sci.*, 10 253–260.

Farid, M.M., & Husaian, R.M. (1990). An electrical storage heater using the phase change method of heat storage. *Energy Conversion and Management*, 30 (3), 219–230.

Farid, M.M., Khudhai, A.M., Razack, S.A.K., & Al-Hallaj, S. (2005). A review on phase change energy storage: materials and applications. *Energy Conversion and Management*, 45 1597–1615.

Gnielinski, V. (1976). New equations for heat and mass transfer in turbulent pipe and channel flow. *Int. Chem. Eng*, 16 359–368.

Hestenes, M.R., & Stiefel, E.L. (1952). *NSB J. Res.*, 49 409 436.

Hawes, D.W., Feldman, D., & Banu, D. (1993). Latent heat storage in building materials. *Energy Buildings*, 20 77–86.

Hepbasli, A., & Akdemir, O. (2004). Energy and exergy analysis of a ground source (geothermal) heat pump system. *Energy Conversion and Management,* 45 737–753

Holman, J.P. (2001). *Experimental Methods For Engineers*. (7th ed.). NewYork: McGraw Hill.

Humphries, W.R., & Griggs, El.A. (1977). A designing handbook for phase change thermal control and energy storage devices. *NASA*, Technical Paper.

Ismail, K.A.R., & Abugderah, M.M. (2000). Performance of a thermal storage system of the vertical tube type. *Energy Conversion and Management*, 41 1165–1190.

Ismail, K.A.R., & Alves, C.L.F. (1986). Analysis of the shell–and–tube PCM storage system. *Proceedings of the 8th International Heat Transfer Conference*, 1781–1786.

Ismail, K.A.R., & Batista de Jesus, A. (2001). Parametric study of solidification of PCM around a cylinder for ice-bank application. *International Journal of Refrigeration*, 24 809–822.

Ismail, K.A.R., & Gonçalves, M.M. (1999). Thermal performance of PCM storage unit. *Energy Conversion and Management*, 40 115–138.

Jekel, T.B., Mitchell, J.W., & Klein S.A. (1993). Modeling of ice–storage tanks, *ASHRAE Trans.*, 99 (1), 1016–1024.

Kays, W.M., & Crawford, M.E. (1980). *Convective Heat and Mass Transfer*, New York: McGraw–Hill.

Lacroix, M. (1993). Study of the heat transfer behaviour of a latent heat thermal energy storage unit with a finned tube. *International Journal of Heat Mass Transfer,* 36 2083–2092.

Lane, G.A. (1986). *Solar Heat Storage: Latent Heat Material*, vol. II. Technology. Florida: CRC Press.

Lane, G.A., Glew, D.N., Clark, E.C., Rossow, H.E., Quigley, S.W., & Drake S.S. (1975). Heat of fusion system for solar energy storage subsystems for heating and cooling of building. Chalottesville, Virginia, USA.

Lee, A.H.W., & Jones, J.W. (1996). Modeling of an ice–on–coil thermal energy storage system. *Energy Conversion and Management*, 37 (10), 1493–1507.

Lee, SL. (1989). A strongly implicit solver for two–dimensional elliptic differential equations. *Numerical Heat Transfer,* 16 161–178.

Lorsch, H.G., Kauffman, K.W., & Denton, J.C. (1976). Thermal energy storage for heating and air conditioning, Future energy production systems. *Heat Mass Transfer Processes*, 1 69–85.

Michels, H., & Hahne, E. (1996). Cascaded latent heat storage process heat. *Proceedings of the 8th International Symposium on Solar Thermal Concentrating Technologies*, Cologne (Germany).

Mulligan, J.C., Colvin, D.P., & Bryant, Y.G. (1996). Microencapsulated phase-change materials suspensions for heat transfer in spacecraft thermal systems. *J. Spacecraft and Rockets*, 33 278–284.

Nelson, D., Vick, B., & Yu, X. (1996). Validation of the algorithm for ice–on–pipe brine thermal storage system. *ASHRAE Trans*., 102 (1), 55–62.

Neto, J.H.M., & Krarti, M. (1997[a]). Deterministic model for an internal melt ice–on–coil thermal energy system. *ASHRAE Trans*., 102 (1), 113–124.

Neto, J.H.M., & Krarti, M. (1997[b]). Experimental validation of a numerical model for an internal melt ice–on–coil thermal storage system. *ASHRAE Trans*., 102 (1), 125–138.

Pal, D., & Joshi, Y. (1997). Application of phase change materials to thermal control of electronic modules: A computation study. *ASME Trans.*, 119 40–50.

Patankar, S.V. (1980). *Numerical Heat Transfer and Fluid Flow*. NY: McGraw-Hill.

Salyer, I.O., & Sircar, A.K. (1990). Phase change materials for heating and cooling of residential buildings and other applications. *Proceedings of the 25th Intersociety Energy Conversion Engineering Conference* - IECEC'90.

Shi. W., Wang, B., & Li, X. (2005). A measurement method of ice layer thickness based on resistance–capacitance circuit for closed loop external melt ice storage tank. *Applied Thermal Engineering*, 25 (11–12), 1697–1707.

Stone, H.L. (1968). Iterative solution of implicit approximations of multidimensional partial differential equations, *SIAM, J. Numer. Anal.*, 5 (3), 530–558.

Thomas, L.H. (1949). Elliptic problems in linear difference equations over a network, *Watson Sci., Compt. Lab. Report*, Columbia University, New York.

Trp, A. (2005). An experimental and numerical investigation of heat transfer during technical grade paraffin melting and solidification in a shell–and–tube latent thermal energy storage unit. *Solar Energy*. 79 (6), 648–660.

Vakilaltojjar, S.M., & Saman, W. (2001). Analysis and modeling of a phase change storage system for air conditioning applications. *Applied Thermal Engineering*, 21 249–263.

Versteeg, H.K., & Malalasekera W., (1995). *An Introduction to Computational Fluid Dynamics: The finite volume method*, London: Prentice Hall.

Zalba, B., Marin, J.M., Cabeza, L.F., & Mehling, H. (2003). Review on thermal energy storage with phase change: materials, heat transfer analysis and applications. *Applied Thermal Engineering*, 23 251–283.

Zhang, Y., & Faghri, A. (1996). Analytical solution of thermal energy storage system with conjugate laminar forced convection. *International Journal of Heat Mass Transfer*, 39 717–724.

Zhu, Y., & Zhang, Y. (2001). Modelling of thermal process for internal melt ice–on–coil tank including ice–water density difference. *Energy and Building* 33 363–370.

APPENDIX

A.1 Formulation of the S.I.S. Solver (Lee, 1989)

Consider a two-dimensional elliptic differential equation to be discretized in the rectangular domain of $x_1 \le x \le x_m$ and $y_1 \le y \le y_n$. Let the domain be divided into $(m-1)\times(n-1)$ rectangular cells with $m \times n$ grid points, that is, (x_i, y_i), $i = 1, 2, \ldots, m$ and $j = 1, 2, \ldots, n$. For convenience, (x_i, y_i) is numbered as the k^{th} point, with $k = (i-1)n + j$ (Figure A.1).

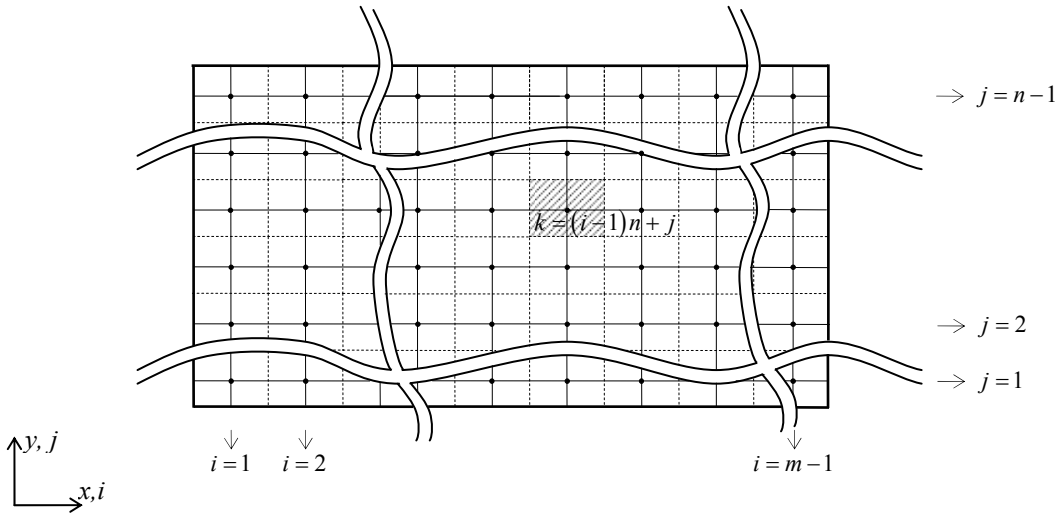

Figure A.1 Computational domain

Upon discretizing the differential equations by using an implicit numerical scheme such as the central difference scheme, the power law scheme, the weighting function scheme or the finite analytical scheme, one obtains a system of $m \times n$ algebraic equations in the form,

$$\begin{aligned}(a_{SW})_k \theta_{k-n-1} + (a_W)_k \theta_{k-n} + (a_{NW})_k \theta_{k-n+1} + (a_S)_k \theta_{k-1} + (a_P)_k \theta_k + (a_N)_k \theta_{k+1} \\ + (a_{SE})_k \theta_{k+n-1} + (a_E)_k \theta_{k+n} + (a_{NE})_k \theta_{k+n+1} \\ = (a_R)_k\end{aligned} \tag{1}$$

where $k = 1, 2, \ldots, m \times n$. Let θ_k^* be a guessed solution and $\alpha_k \theta_{k-n-1} = \alpha_k \theta_{k-n+1}^*$ and $\beta_k \theta_{k+n-1} = \beta_k \theta_{k+n-1}^*$ be added into Equation (1). This leads to,

$$[M]\{\theta\} = \{N\} \tag{2}$$

where, $[M]$ is a *nine-diagonal* coefficient matrix and both $\{\theta\}$ and $\{N\}$ are $m \times n-$ dimensional column vectors. It is important to note that there uniquely exists a set of $\alpha_k, \beta_k, k = 1, 2, \ldots, m \times n$, such that the matrix $[M]$ can be factored into the products of a lower triangular matrix $[L]$ and an upper one $[U]$, that is,

$$[M] = [L][U] \tag{3}$$

where both $[L]$ and $[U]$ possess only nonzero diagonals as shown in Figure A.2. Let A_k, B_k, C_k and D_k be the four nonzero diagonals of $[L]$ and 1, E_k, F_k, and G_k be those of $[U]$.

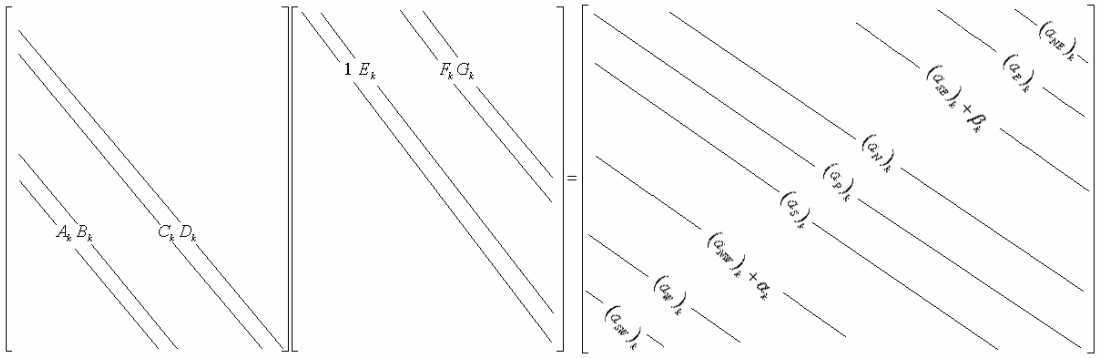

Figure A.2 Schematic representation of the lower $[L]$ and upper $[U]$ triangular matrices and their product matrix $[M]$

The relationship between the elements of $[L]$ $[U]$ and $[M]$ thus is expressible as,

$$
\begin{aligned}
&A_k = (a_{SW})_k \\
&A_k E_{k-n-1} + B_k = (a_W)_k \\
&B_k E_{k-n} = (a_{NW})_k - \alpha_k \\
&A_k F_{k-n-1} + C_k = (a_S)_k \\
&A_k G_{k-n-1} + B_k F_{k-n} - C_k E_{k-1} + D_k = (a_P)_k \\
&B_k G_{k-n} + D_k E_k = (a_N)_k \\
&C_k F_{k-1} = (a_{SE})_k - \beta_k \\
&C_k G_{k-1} + D_k F_k = (a_E)_k \\
&D_k G_k = (a_{NE})_k
\end{aligned}
\tag{4}
$$

Solving the nine unknowns A_k, B_k, C_k, D_k, E_k, F_k, G_k, α_k and β_k from the nine algebraic Equations (4), one gets,

$$
\begin{aligned}
&A_k = (a_{SW})_k \\
&B_k = (a_W)_k - A_k E_{k-n-1} \\
&C_k = (a_S)_k - A_k F_{k-n-1} \\
&\alpha_k = B_k E_{k-n} - (a_{NW})_k \\
&\beta_k = C_k F_{k-1} - (a_{SE})_k \\
&D_k = (a_P)_k - A_k G_{k-n-1} - B_k F_{k-n} - C_k E_{k-1} \\
&E_k = \frac{(a_N)_k - B_k G_{k-n}}{D_k} \\
&F_k = \frac{(a_E)_k - C_k G_{k-1}}{D_k}
\end{aligned}
\tag{5}
$$

$$G_k = \frac{(a_{NE})_k}{D_k}$$

Now, with the particular values of α_k and β_k defined in Equation (5), the elements of the column vector $\{N\}$ can be determined from,

$$H_k = (a_R)_k + \alpha_k \theta^*_{k-n+1} + \beta_k \theta^*_{k+n-1} \tag{6}$$

In summary, for a large set of algebraic equations in the form of Equation (1), one may factor the coefficient matrix $[M]$ into product of $[L]$ and $[U]$ by using Equation (5). Next, guess a solution field for θ^*_k, $k = 1, 2, \ldots, m \times n$, and evaluate the vector $\{N\}$ from Equation (6). The solution then is renewed by solving the equations,

$$\begin{aligned} [L]\{\phi\} &= \{N\} \\ [U]\{\theta\} &= \{\phi\} \end{aligned} \tag{7}$$

Let $\theta_{k,new}$ be the new solution obtained from equation (7) and $\theta_{\max}$ and $\theta_{\min}$ be the maximum and minimum values of $\theta_{k,new}$. If the solution $\theta_{k,new}$ agrees with the guessed one θ^*_k within a prescribed tolerance TOL, that is,

$$\underset{k=1,2,\ldots m\times n}{Max} \left| \frac{\theta_{k,new} - \theta^*_k}{\theta_{\max} - \theta_{\min}} \right| \le TOL \tag{8}$$

the solution $\theta_{k,new}$ will be regarded as the converged solution. Otherwise, the procedure should be repeated until criterion (8) is satisfied. For a better convergence rate, the guessed solution θ^*_k is modified by employing a successive over-relaxation factor SOR in the manner,

$$\theta^*_{k,new} = \theta^*_k + SOR\left(\theta_{k,new} - \theta^*_k\right) \tag{9}$$

for the next iteration.

It is noted that the $L-U$ factorization procedure (5) needs to be performed only once, even though a change in the value of SOR is desired from one iteration to another. To converse the storage, the values of $\left(a_{SW}\right)_k$, $\left(a_W\right)_k$, $\left(a_{NW}\right)_k$, $\left(a_S\right)_k$, $\left(a_P\right)_k$, $\left(a_N\right)_k$, $\left(a_{SE}\right)_k$, $\left(a_E\right)_k$ and $\left(a_{NE}\right)_k$ can be replaces, respectively, by A_k, B_k, α_k, C_k, D_k, E_k, β_k, F_k and G_k, through Equation (5).